International Journal of Earth Sciences (2022) 111:1129–1148
https://doi.org/10.1007/s00531-022-02160-x

ORIGINAL PAPER

Internal igneous growth, doming and rapid erosion of a mature ocean island: the Miocene evolution of Maio (Cabo Verde)

Lisa K. Samrock[1] · Thor H. Hansteen[1] · Wolf-Christian Dullo[1] · Jo-Anne Wartho[1]

Received: 22 July 2021 / Accepted: 10 January 2022 / Published online: 17 March 2022

Abstract

Maio Island (Cabo Verde Archipelago) is composed of uplifted Early Mesozoic MORB-type pillow lavas and deep-sea sediments, unconformably overlain and intruded by Miocene igneous rocks. Combined structural analyses and ^{40}Ar–^{39}Ar dating were used to constrain the Miocene evolution of Maio. Structures and ages of uplifted Mesozoic sequences and crosscutting Miocene dykes showed that numerous intrusive events were associated with the intense growth of an igneous core complex in the middle to upper crust, causing semi-circular doming and partial disruption of the Mesozoic strata. Two nosean nephelinite dykes cut the Valanginian Batalha Formation and yielded phlogopite ^{40}Ar–^{39}Ar ages of 10.405 ± 0.033 Ma and 10.570 ± 0.053 Ma (2σ errors). A nosean nephelinite dyke that cuts the overlying Valanginian to Early Aptian Morro Formation yielded an age of 9.273 ± 0.020 Ma. Combined with existing K–Ar and ^{40}Ar–^{39}Ar ages, this confirmed a main period of island growth between ~ 16 and 8.7 Ma. We re-interpreted extensive polymict conglomerates, which occur below the Late Miocene Monte Penoso Formation, as landslide deposits. A nephelinite lava clast yielded a phlogopite ^{40}Ar–^{39}Ar age of 8.666 ± 0.0274 Ma, which represents a maximum age for these landslides and thus confined a period of large-scale flank collapses and erosion to between 8.7 and 6.7 Ma. Flank collapses and further mass wasting during this period may have rejuvenated the igneous activity, i.e., resulting in the formation of the Tortonian/Messinian Monte Penoso and Malhada Pedra Formations, due to decompression-induced melting at upper mantle depths. Such interaction between flank collapses and rejuvenated volcanism may be a key to better understand ocean island evolution worldwide.

Keywords ^{40}Ar–^{39}Ar dating · Ocean island volcanism · Doming · Flank collapse · Cabo Verde

Introduction

Volcanic ocean islands show a typical pattern of growth stages, starting with a submarine seamount stage, followed by a shield building stage, collapse of parts of the shield volcano, final volcanism during a rejuvenation stage, and in many cases the final guyot phase (Clague and Dalrymple 1987). The volcanic Cabo Verde Archipelago hosts islands and seamounts in various growth stages, ranging from the seamount stage (e.g., Cadamosto Seamount; Samrock et al. 2019), to the rejuvenation stage (e.g., São Vicente; Ancochea et al. 2010). Maio Island, situated in the E of the archipelago, is one of the oldest islands in the archipelago and is volcanically inactive (Fig. 1).

✉ Lisa K. Samrock
lsamrock@geomar.de

[1] GEOMAR Helmholtz Centre for Ocean Research Kiel, Wischhofstr. 1–3, 24148 Kiel, Germany

Large-scale landslides or the collapse of island flanks are typical for volcanic edifices and have a large hazard potential, especially if associated with catastrophic tsunamis (Masson et al. 2008; Watt et al. 2014; Ramalho et al. 2015; van Wyk de Vries and Davies 2015; Madeira et al. 2020). Several landslide and collapse events have been discovered in the Cabo Verde Archipelago, for example, on Santo Antão and Fogo (Masson et al. 2008; Ramalho et al. 2015; Day et al. 1999). The interplay between volcanic growth and destruction by flank collapses is still poorly understood (Cornu et al. 2021).

Similar to the neighbouring island of Boa Vista, Maio is deeply eroded and mostly dominated by gentle hills, with only a few topographic highs up to 436 m in elevation (e.g., Monte (Mte) Penoso; Figs. 1, 2). Maio comprises a basement of uplifted Mesozoic mid-ocean ridge basalt (MORB) lavas and dykes (Batalha Formation). Cretaceous deep-sea sedimentary rocks (Morro and Carqueijo Formations) are overlain by a series of Miocene to Pliocene volcanic rocks and

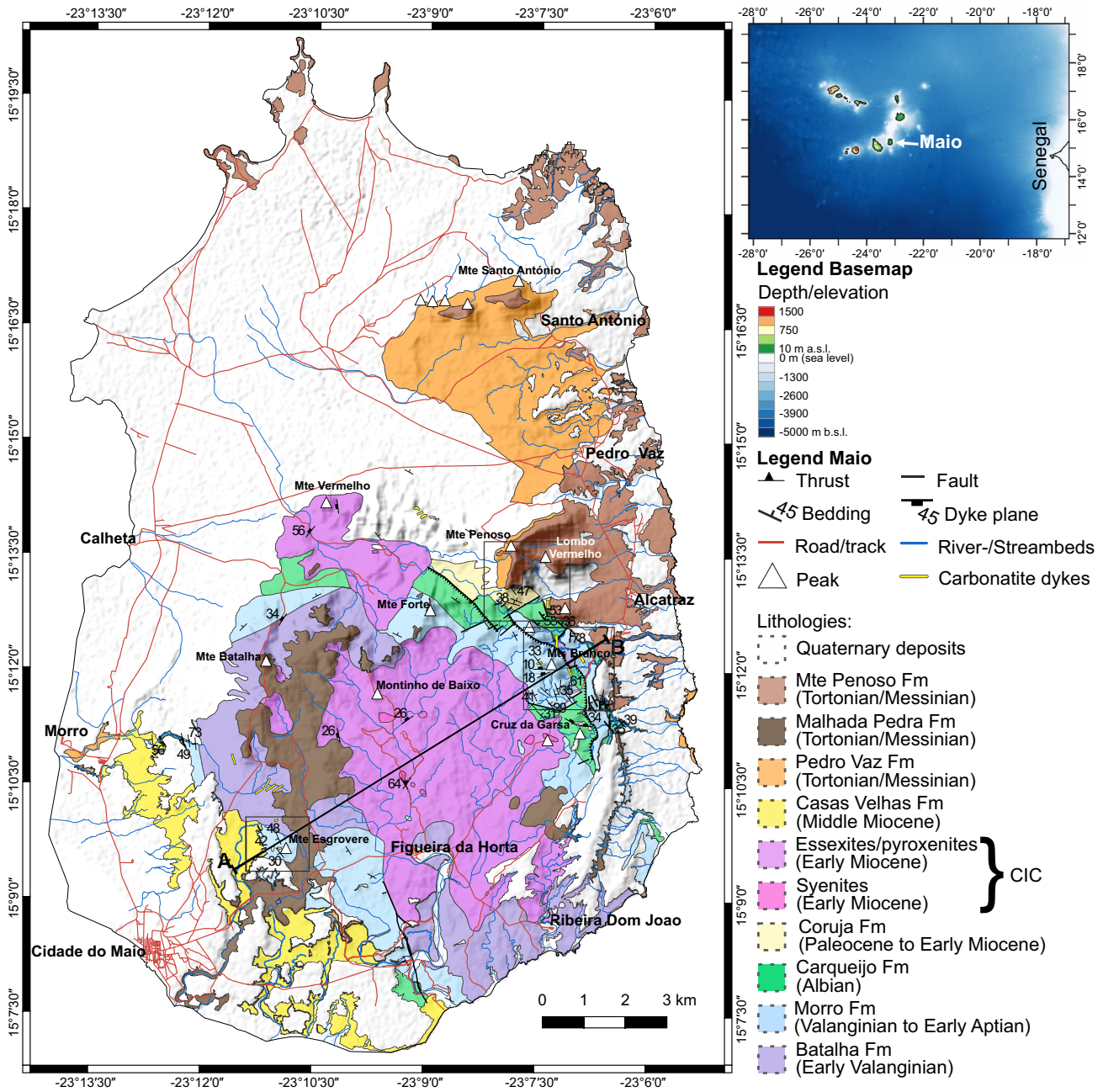

Fig. 1 Geological map of Maio, modified after Serralheiro (1970) and Stillman et al. (1982), including our new field observations and mapping. The topographical shading is based on Shuttle Radar Topography Mission (SRTM) data, and the basemap is from OpenStreetMap. The black line (**A**, **B**) marks the profile shown in Fig. 2a, and the black boxes indicate areas enlarged in Fig. 2b–d. Top right: Insert map of the Cabo Verde Archipelago, showing the location of Maio (bathymetry data from General Bathymetric Chart of the Oceans (GEBCO) and topography data from SRTM)

conglomerates of the Casas Velhas, Pedro Vaz, Malhada Perdra and Mte Penoso Formations and are partially displaced by the Miocene Central Intrusive Complex (CIC) (Paepe et al. 1974; Stillman et al. 1982; Fig. 1). Large volumes of the Miocene volcanic rocks are eroded, exposing the uplifted seafloor and intrusive basement of the island. The Miocene evolution and processes of doming, collapse and erosion on Maio are still debated and poorly understood, although this deeply eroded island allows the study of different phases of growth, intensive erosion and collapse in great detail.

During two field campaigns on Maio in 2017 and 2018, we found new evidence for an intense erosive phase, predating the youngest volcanic activity on Maio. In this study, we present new field observations of the Miocene intrusive and erosive units, their structural and stratigraphical relationships, and new ^{40}Ar–^{39}Ar ages. This allows re-evaluation of

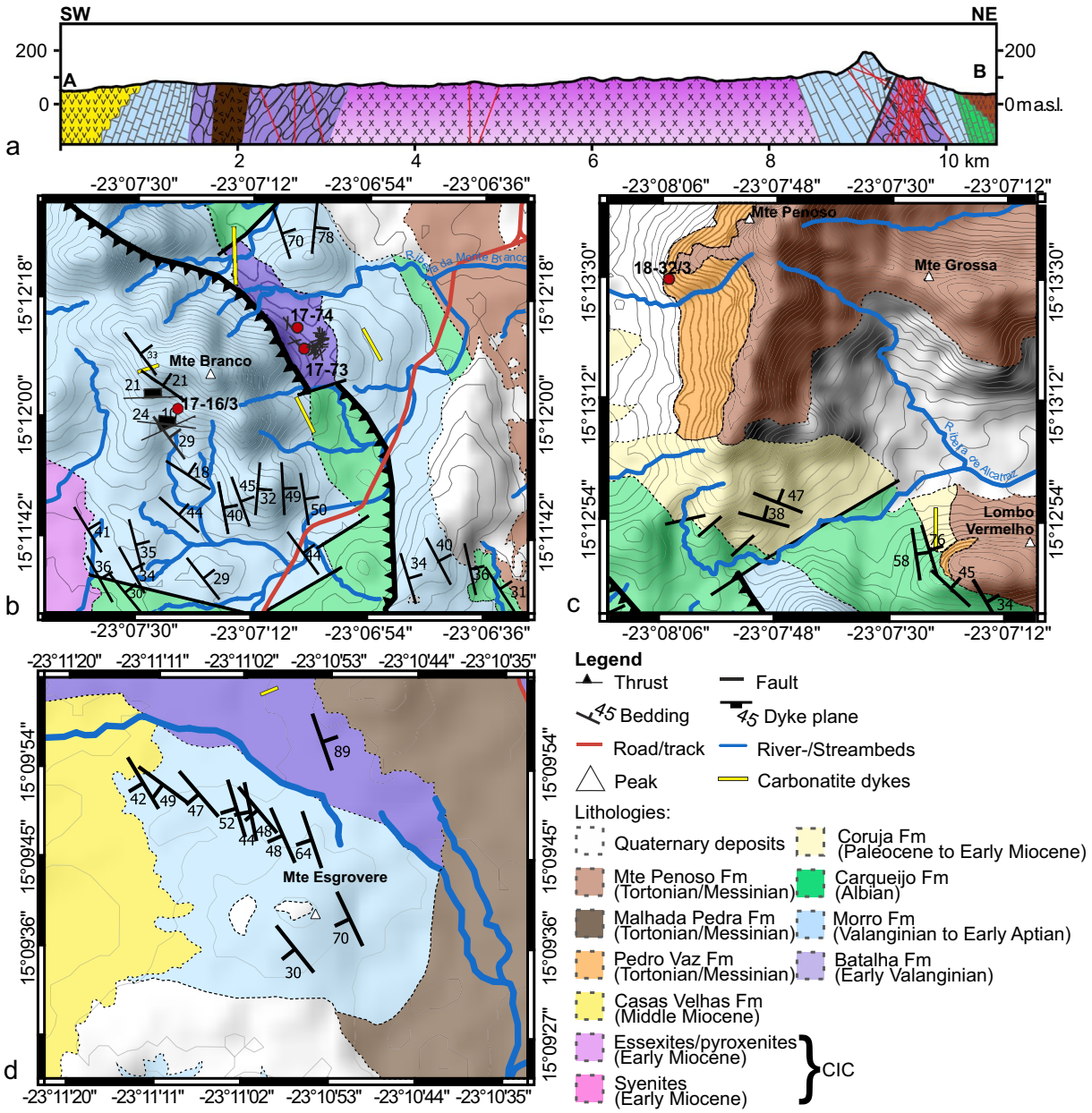

Fig. 2 Geological profile across Maio (**a**) and enlargements from Fig. 1 geological map (**b**–**d**). Sampling locations and dykes intruding the Batalha Formation below the Mte Branco Thrust (**b**), the study locations for the conglomerate below Mte Penoso Formation rocks (**c**), and enlarged image of the Mte Esgrovere area in the SW (**d**). Red circles = ^{40}Ar–^{39}Ar sampling locations

the ages of intrusive growth of the island, phases of erosion and collapse, and structural processes that shaped the current topography on Maio. In addition, we present a refined model of the stratigraphy and geological evolution of Maio.

Geological setting

The Cabo Verde Archipelago, which comprises 10 islands, several islets and seamounts in two volcanic chains, is situated on one of Earth's most prominent bathymetric anomalies, the Cape Verde Rise (Fig. 1). It rises ~ 2000 m from the surrounding seafloor and is associated with geoid, gravity, and thermal anomalies that are thought to originate in the deep mantle (Dash et al. 1976; Crough 1982; Courtney and White 1986; Ali et al. 2003; Pim et al. 2008; Wilson et al. 2010). The archipelago has been volcanically active since the Oligocene, with the oldest subaerial volcanic activity reported from Sal at ~ 26 Ma (Torres et al. 2002).

The eastern islands in both volcanic chains are deeply eroded, while the western islands have higher topographies (e.g., Ramalho

et al. 2010a). Maio is located on the seafloor between paleomagnetic Chrons M11 (~136 Ma) and M16 (~141 Ma; Gradstein 2012). The islands show a flexural moat due to volcanic loading that has been filled with sediments, which are tilted away from the islands due to uplift of the edifices (Ali et al. 2003).

The geological units on Maio have been mapped by Serralheiro (1970) and further refined and named by Stillman et al. (1982). The oldest rocks on Maio are MORB-type pillow lavas and dykes of the Early Cretaceous (Valanginian) Batalha Formation (Paepe et al. 1974; Stillman et al. 1982; Robertson 1984; Casson et al. 2020). The upper part of the Batalha Formation contains intercalated sediments that include Early Valanginian calpionellids (Azéma et al. 1990; Fourcade et al. 1990; Casson et al. 2020).

The Batalha Formation rocks are overlain by Cretaceous siliceous pelagic nannofossil limestones and marls of the Morro Formation (Valanginian to Barremian/Early Aptian), which were formed in a deep-sea environment (Figs. 1, 2, 3). Based on the assemblages of macrofossils (e.g., ammonites and aptychi) and nannofossils (e.g., radiolaria and *Nannoconus*) the Morro Formation is attributed to the Maiolica facies (Stahlecker 1934; Robertson and Bernoulli 1982; Robertson 1984; Casson et al. 2020). The Albian Carqueijo Formation appears to conformably overlie the Morro Formation sequences; however, biostratigraphic analyses suggest a hiatus between these formations (Fig. 3; Robertson 1984; Casson et al. 2020). The Carqueijo Formation is seen as the equivalent to Mid-Cretaceous black shale deposits in the Central Atlantic Ocean (Fig. 1; Stillman et al. 1982; Robertson 1984; Fourcade et al. 1990; Casson et al. 2020). All these Cretaceous units formed on the seafloor prior to island formation, underwent uplift, and now form a circular structure dipping away from the Miocene CIC. Thrusting results in local repetition of the Cretaceous sedimentary units, especially in the NE of Maio (Monte Branco area; Robertson and Bernoulli 1982).

The CIC contains alkaline, silica-undersaturated rocks (essexites, pyroxenites, syenites and some carbonatites; Figs. 1, 2; Serralheiro 1970; Stillman et al. 1982). The Batalha Formation, limestones of the Morro Formation, the Carqueijo Formation, and the CIC form the Basement Complex (Fig. 3; Stillman et al. 1982).

Intrusive and volcanic activity on Maio started at ~19 Ma with the formation of the CIC and dyke intrusions in the Cretaceous sedimentary rocks (Mitchell et al. 1983). The Mesozoic units of the Basement Complex are apparently conformably overlain by volcaniclastic sediments (tuffs, sandstones, and conglomerates) of the Coruja Formation (Figs. 1, 2, 3; Stillman et al. 1982; Robertson 1984). Although rare planktonic foraminifera suggest a Paleocene to Early Miocene age for the Coruja Formation, it is difficult to determine the onset of extrusive volcanism on Maio (Robertson 1984; Bernoulli et al. 2007). The formations of the Basement Complex are unconformably overlain by ankaramite lavas of the subaerial Miocene Casas Velhas Formation, in the SW of Maio, and by sedimentary and volcaniclastic units of the Pedro Vaz Formation in the NE of Maio (Fig. 3; Serralheiro 1970; Stillman et al. 1982). The Casas Velhas Formation is dated by K–Ar at 9.8 ± 0.8 Ma (all errors are quoted at the 2σ level; Mitchell et al. 1983), and by ^{40}Ar–^{39}Ar at 11.9 ± 1.0 Ma (Ramalho 2011). Volcanic activity continued with the eruption of Malhada Pedra lava flows, dated by K–Ar at 7.3 ± 0.4 Ma and 6.5 ± 1.2 Ma, and the formation of the Monte Penoso stratovolcano, dated by K–Ar at 6.9 ± 0.4 and 6.7 ± 0.4 Ma (Fig. 3; Stillman et al. 1982; Mitchell et al. 1983). The remnants of this volcano now form the highest elevation on the island, at ~436 m above sea level (a.s.l.). Extensive Pliocene and Quaternary marine terraces, with elevations up to 100 m a.s.l., cover large areas, especially on the coastal regions of Maio. These marine terraces occur at different elevation levels and suggest several phases of uplift and subsidence (Serralheiro 1970; Ramalho et al. 2010a; Samrock et al. 2018). The coastal areas of Maio additionally exhibit numerous Pleistocene tsunami deposits (Madeira et al. 2020).

Methods

This study integrated field observations with ^{40}Ar–^{39}Ar geochronology and structural analyses. Structural measurements were taken with the Lambert App (Appel 2017), quoted with dip direction/dip angles. Structural plots were created with Stereonet v.11 (Allmendinger et al. 2012; Cardozo and Allmendinger 2013).

Phlogopite crystals from three dyke samples within the Morro and Batalha Formations, and phlogopite from a nephelinite lava clast in a conglomerate from the landslide deposits directly below Mte Penoso were dated using the ^{40}Ar–^{39}Ar technique. The ^{40}Ar–^{39}Ar sample locations are detailed in Table 1 (Figs. 2, 3, 4, 5). Sample descriptions are summarized in Appendix A. The samples were prepared for dating by crushing, sieving and washing in distilled water in an ultrasonic bath. Phlogopite separates in the 0.25–0.5 mm and 0.5–1 mm size fractions were separated and handpicked under a binocular microscope, and cleaned in acetone before drying in an oven at 50 °C overnight. The samples were loaded into an aluminum cannister, and irradiated with fast neutrons in a Cadmium-Lined In-Core Irradiation Tube (CLICIT) reactor for four hours at the Oregon State University nuclear reactor, Corvallis, USA. The samples were analyzed at the GEOMAR Argon Geochronology in Oceanography (ArGO) Laboratory in Kiel, Germany. The isotopic analyses were corrected using the total K decay constant and atmospheric air ratio of Steiger and Jäger (1977); using the recommendation of Fleck et al. (2019), and *J* values were determined using the Taylor Creek sanidine (TCR-2) age standard (28.344 ± 0.0114 Ma, 1σ; Fleck et al. 2019).

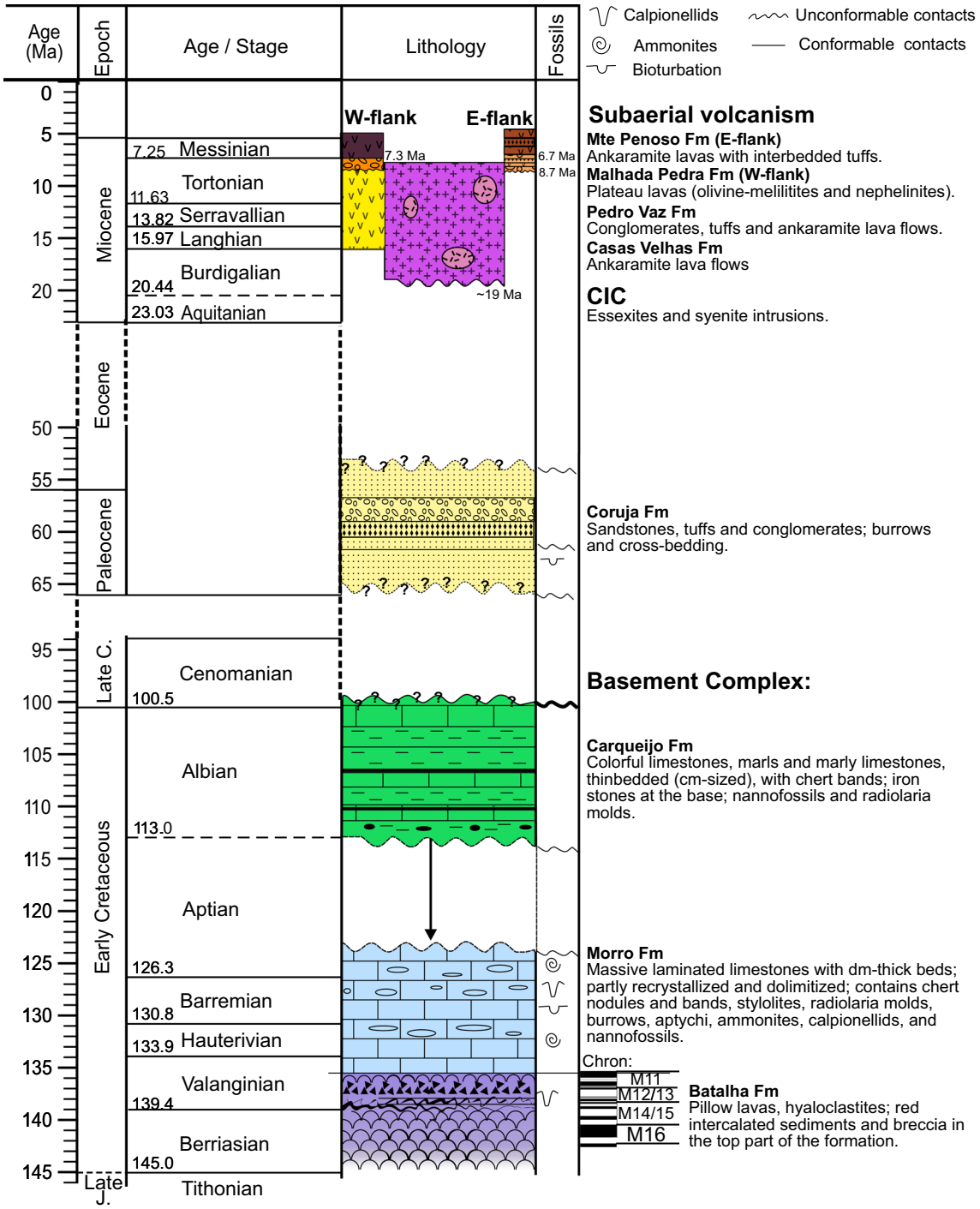

Fig. 3 Simplified stratigraphic column of the Maio sequences, separated by the eastern and western flanks of Maio. K–Ar and ^{40}Ar–^{39}Ar ages for the Miocene formations are notated in the lithology and fossil columns and were based on this study and data from Bernard-Griffiths et al. (1975) and Mitchell et al. (1983). The geological timescale and Chrons were modified after Gradstein (2012). The arrow between the Morro and Carqueijo Formations indicates a hiatus of apparently conformably overlying rocks

A summary of the ^{40}Ar–^{39}Ar data are shown in Table 2, and the full ^{40}Ar–^{39}Ar data are shown in Appendix B. All our ^{40}Ar–^{39}Ar ages in the text and figures are quoted with 2σ internal errors, and include analytical, *J* value, and irradiation correction factor errors. A complete description of the laser step-heating and single-/multi-grain laser total fusion ^{40}Ar–^{39}Ar methods are given in Samrock et al. (2019).

Table 1 Sample numbers and location coordinates of samples dated by the ^{40}Ar–^{39}Ar technique

Sample #	Sample type	Sampling location	Sampling coordinates	
			Latitude	Longitude
17–16/3	Nosean nephelinite dyke in Morro Formation limestones	SW-flank of Mte Branco	15.200262	−23.123276
17–73	Nephelinite dyke in Batalha Formation pillow lavas	NE of Mte Branco	15.202839	−23.117849
17–74	Nephelinite dyke in Batalha Formation pillow lavas	NE of Mte Branco	15.203719	−23.118145
18–32/3	Nosean nephelinite clast in Pedro Vaz Formation conglomerate	SW-flank of Mte Penoso	15.224898	−23.134683

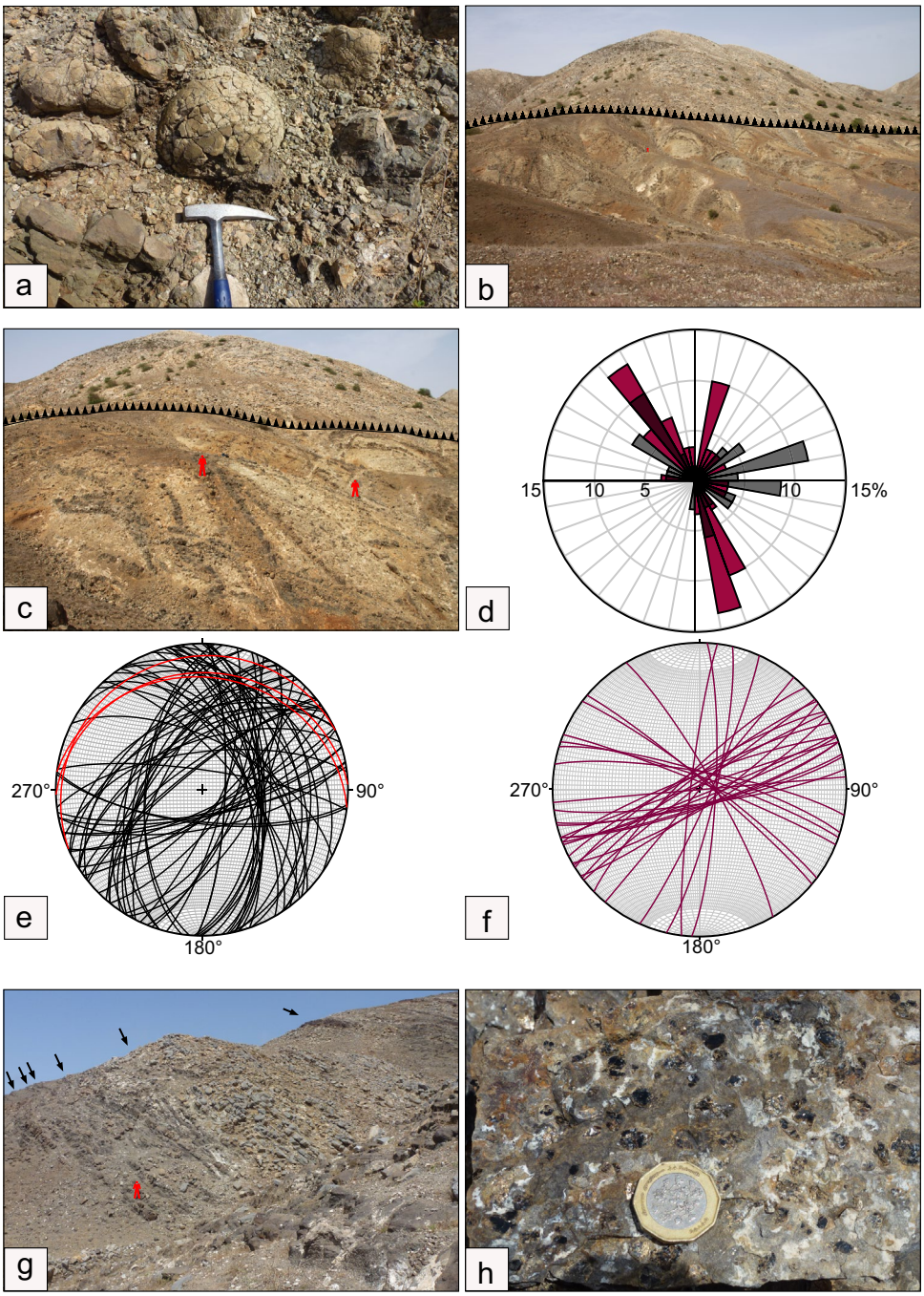

Fig. 4 Dyke intrusions in the Basement Complex. Rocks of the Batalha Formation (pillow lavas; **a**) were heavily intruded by dykes that were truncated by the Mte Branco Thrust (**b**–**c**). Rose diagram (**d**) of the dip directions of the dykes: Almost vertical dykes (≥ 80°, $n = 30$) dip towards the NW, NNE and SSE; while all the other dykes (with dips of 25–79°, $n = 70$) show an additional group of ENE and southward dipping dykes. Stereoplots of dykes intruding the Batalha Formation, separated by moderate (25–79°, $n = 70$; **e**) and high (≥ 80°, $n = 30$; **f**) dip angles, showing a slight dominance in the NE–SW and NNE–SSW trends. The Morro Formation limestones at Mte Branco are also intruded by undulating dykes (**g**). A phlogopite-bearing sample (17–16/3) was used for ^{40}Ar–^{39}Ar dating (**h**). A hammer (**a**), red people (**b**, **c** and **g**) and coin (**h**) are shown for scale

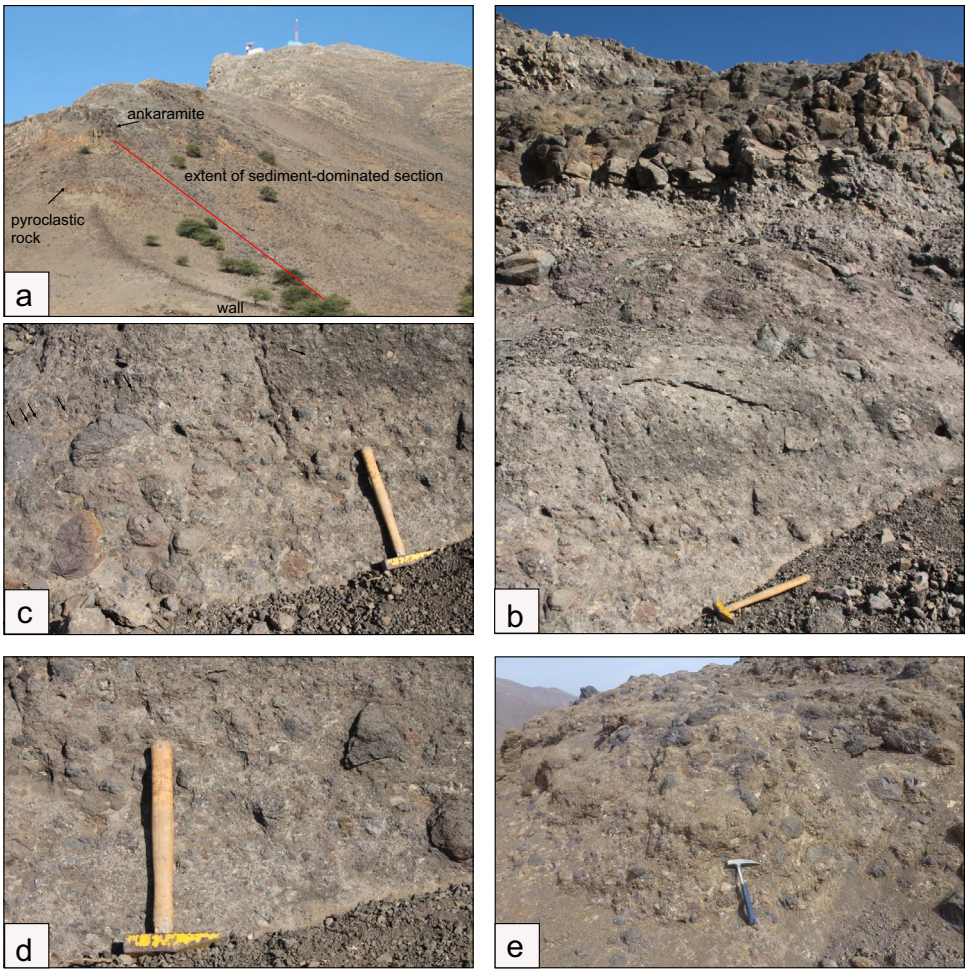

Fig. 5 Polymict conglomerates crop out at the base of Mte Penoso (**a**–**d**) and at Lombo Vemelho (**e**). The successions record multiple mass wasting and pyroclastic events, indicated by local lenticular pyroclastic units (**a**). The conglomerate successions are overlain by ankaramite lava flows of the Mte Penoso Formation (**a**). Clasts are well rounded to angular, vary in grain sizes from cm to dm in diameter, and are composed of various lithologies, including alkali-basalt, ankaramite, phonolite lava and alkaline plutonic rocks (**b**–**d**). At Lombo Vermelho (**e**), fragments of the Mesozoic limestone units are also found. These clasts are poorly sorted and set in a matrix that shows signs of hydrothermal alteration. The conglomerate varies between matrix- and clast-supported textures (**b**–**e**)

The ^{40}Ar–^{39}Ar corrections, age determinations, and plateau and inverse isochron plots were made using the ArArCALC Excel macro (v. 2.5.2) developed by Koppers (2002). The single-crystal total-fusion weighted mean plots were obtained using the Excel Isoplot macro v. 4.15 (Ludwig 2011), and the ^{40}Ar–^{39}Ar data and plots are presented in Appendix B. Plateau ages were determined using the criteria of Lanphere and Dalrymple (1978), where the plateau was comprised of at least 3 consecutive heating steps that were within 2σ errors of each other, and where a significant proportion of the ^{39}Ar release (> 50%) is represented in the plateau steps. ^{36}Ar/^{39}Ar alteration index (AI) values were used as a guide to gauge the alteration/freshness of the phlogopite samples, calculated using the criteria of Baksi (2007), with a cut-off value of ^{36}Ar/^{39}Ar AI < 0.0013 for the single-/multi-crystal total-fusion analyses, and < 0.0005 for the step-heated samples.

Results

In the following section, we (a) present field observations from the Pre-Miocene Basement Complex and the Miocene sequences, and (b) combine the structural relationships for four dykes intruded into the Basement Complex at two key locations (see Fig. 2b, c) with new ^{40}Ar–^{39}Ar data (Table 2). In addition, we (c) describe a newly discovered mass wasting deposit, which we ascribe to the Mid- to Late Miocene Pedro Vaz Formation.

Field observations

Pre-Miocene Basement Complex

The Basement Complex comprises Early Cretaceous pillow lavas of the Batalha Formation, the Early Cretaceous pelagic limestones of the Morro and Carqueijo Formations,

Table 2 Summary of the Maio single-/multi-crystal total fusion and step-heating ^{40}Ar–^{39}Ar ages

Sample #	Sample type	Material/size fraction	Laboratory						n = steps/analyses
			ID #	Age ± 2σ (Ma)	Analyses/age type	% ^{39}Ar	MSWD	*P* %	
17–73	Nephelinite dyke in Batalha Formation	Phlogopite (0.25–0.5 mm)	1773b	10.61 ± 0.13	SH—High-T WMA	18.7	4.39	*0*	15–20
17–73	Nephelinite dyke in Batalha Formation	Phlogopite (0.25–0.5 mm)	1773b	**10.570 ± 0.053**	SCTF/MCTF—WMA	–	1.49	8	20 of 24
17–74	Nephelinite dyke in Batalha Formation	Phlogopite (0.5-1 mm)	1774b	10.466 ± 0.070	SH—High-T WMA	29.9	1.94	7	14–20
17–74	Nephelinite dyke in Batalha Formation	Phlogopite (0.5-1 mm)	1774b	**10.405 ± 0.033**	SCTF—WMA	–	1.12	32	22 of 24
17–16/3	Nosean nephelinite dyke in Morro Formation	Phlogopite (0.25–0.5 mm)	163bs	9.263 ± 0.024	SH—Plateau	100.0	1.22	23	1–20
17–16/3	Nosean nephelinite dyke in Morro Formation	Phlogopite (0.25–0.5 mm)	163bs	9.292 ± 0.028	SCTF—WMA	–	1.31	15	24 of 24
17–16/3	Nosean nephelinite dyke in Morro Formation	Phlogopite (0.5–1 mm)	163bl	9.268 ± 0.028	SCTF—WMA	–	0.88	62	23 of 23
17–16/3	Nosean nephelinite dyke in Morro Formation	Phlogopite (0.25–1 mm)	163bs and 163bl	9.282 ± 0.022	SCTF—WMA	–	1.13	26	47 of 47
17–16/3	Nosean nephelinite dyke in Morro Formation	Phlogopite (0.25–1 mm)	163bs and 163bl	**9.273 ± 0.020***	Combined SCTF/SH*	–	1.17	16	67
18–32/3	Nosean nephelinite clast in Pedro Vaz Formation	Phlogopite (0.25–0.5 mm)	323bs	8.707 ± 0.045	SCTF—WMA	–	1.18	30	11 of 12
18–32/3	Nosean nephelinite clast in Pedro Vaz Formation	Phlogopite (0.5–1 mm)	323bl	8.654 ± 0.029	SCTF—WMA	–	1.42	12	18 of 24
18–32/3	Nosean nephelinite clast in Pedro Vaz Formation	Phlogopite (0.25–1 mm)	323bs and 323bl	**8.666 ± 0.027**	SCTF—WMA Group 1	–	1.48	5	29 of 36
18–32/3	Nosean nephelinite clast in Pedro Vaz Formation	Phlogopite (0.25–1 mm)	323bs and 323bl	8.825 ± 0.062	SCTF—WMA Group 2	–	*0.19*	83	3 of 36
18–32/3	Nosean nephelinite clast in Pedro Vaz Formation	Phlogopite (0.25–1 mm)	323bs and 323bl	9.68 ± 0.13 to 11.75 ± 0.34	SCTF—Group 3	–	–	–	4 of 36

Table 2 (continued)

Sample #	Inverse isochron		MSWD	*P* %	SF %	n/Steps	% radiogenic	Wt% K	Analyses/steps with	Details
	Age ± 2σ (Ma)	Initial $^{40}Ar/^{36}Ar$					^{40}Ar range	(from $^{39}Ar_K$)	fresh material	
17–73	10.78 ± 0.31	236 ± 102	4.48	0	*7.6*	15–20	26–97	5.9	3–20	Staircase age spectrum, some fresh material
17–73	10.572 ± 0.086	295 ± 18	1.57	6	*23.9*	20	73–98	5.4–9.4	23	Excluding 4 youngest ages (8.95–9.61 Ma), some fresh material
17–74	10.42 ± 0.11	326 ± 56	1.79	11	*20.8*	14–20	14–98	6.0	5–20	Staircase age spectrum, some fresh material
17–74	10.414 ± 0.046	294.2 ± 4.9	1.16	28	41.8	22	55–96	5.9–7.1	22	Excluding 2 youngest ages (9.70–10.15 Ma)
17–16/3	9.270 ± 0.029	292.77 ± 5.9	1.23	22	86.5	1–20	10–98	5.9	4–20	Staircase age spectrum, some fresh material
17–16/3	9.241 ± 0.049	311 ± 13	1.06	39	*25.8*	24	71–95	5.5–7.0	24	All fresh material
17–16/3	9.246 ± 0.040	300.3 ± 6.1	0.81	71	*39.7*	23	58–97	3.8–10.0	23	All fresh material
17–16/3	9.260 ± 0.031	301.1 ± 5.4	1.05	37	*39.7*	47	58–97	3.8–10.0	47	All fresh material
17–16/3	–	–	–	–	–	–	–	3.8–10.0	67	All fresh material
18–32/3	8.706 ± 0.077	296 ± 17	1.31	22	*22.2*	11	73–95	6.2–7.9	12	Excluding 1 oldest age (10.89 Ma), all fresh material
18–32/3	8.659 ± 0.056	294 ± 18	1.51	9	*14.8*	18	81–96	3.0–6.3	24	Excluding 6 oldest ages (8.81–11.75 Ma), all fresh material
18–32/3	8.661 ± 0.046	297 ± 13	1.53	*4*	*23.0*	29	73–96	5.6–7.9	36	Excluding Groups 2 and 3 ages, all fresh material
18–32/3	8.80 ± 0.13	301 ± 23	*0.17*	68	*14.7*	3	79–93	5.5–6.3	3	Excluding Groups 1 and 3 ages, all fresh material
18–32/3	–	–	–	–	–	–	54–63	3.0–4.5	4	Excluding Groups 1 and 2 ages, all fresh material

Numbers in italics indicate statistically invalid values (i.e., MSWD < 0.3 (overestimated error); $P < 5\%$, and SF = < 40%)

Values in bold indicate preferred ages

ID # identification number, *SH* step-heating, *SCTF* single crystal total-fusion, *MCTF* multi-crystal total-fusion (2 grains maximum), *High-T* high-temperature, *WMA* weighted mean age, *MSWD* mean square weighted deviation, *P* probability, *SF* spreading factor, *Wt%* weight %

*The combined SCTF/SH weighted mean age for sample 17-16/3 was calculated using the $^{40}Ar^*/^{39}Ar$ ratios, after the approach of Heath et al. (2018), and includes the analytical and *J* value errors

the probably Paleocene to Eocene Coruja Formation, and the Miocene CIC. The Batalha Formation pillow lavas are exposed along the southern coast of Maio and north of Mte Esgrovere, plus at the western flanks of Mte Batalha and in a small sliver exposed on the NE flank of Mte Branco (Figs. 1, 2). North of Mte Esgrovere, red ferrigenous sediments are found intercalated with the pillow lavas in the upper part of the Batalha Formation, and these sediments are strongly folded and dip vertically (89°). A sample from these intercalated sediments contains a dense, hematite-dominated band and a pelagic protozoan amphore-shaped fossil ?*Calpiollenites darderi* (Colom 1934) Colom 1948, which confirms similar findings by Azéma et al. (1990), Fourcade et al. (1990) and Casson et al. (2020; Appendix C). In the upper part of the Batalha Formation in the Mte Esgrovere area, additional breccias are observed above the

red intercalated sediments that contain angular fragments and altered sedimentary rocks, which may have originated from the underlying red sediments (Fig. 3; Appendix C). Brecciation of lithified sediments during magmatic growth of the Batalha Formation suggests that MORB-type magmatic activity in this area covered a considerable time span.

The limestones of the Morro and Carqueijo Formations are observed in some of the hills surrounding the CIC, e.g., Mte Branco and Mte Carqueijo to the NE and N, respectively (Fig. 1). Limestone beds are tilted away from the CIC, seemingly uplifted and tilted by CIC intrusions during the Miocene, and dip towards the NE at Mte Branco, SW at Mte Esgrovere, W at Ribeira (Rib) do Morro, and E at Rib da Baia (Figs. 1, 2). At Mte Esgrovere, the units dip with an average value of 49° towards the SW, but dip angles are steeper (up to 70°) closer to the CIC (Fig. 2d). At Rib do Morro in the W, the units have an average dip angle of 51°, but numerous meter-scale upright folds are observed with fold axes trending to the SE. At the top of Mte Branco, the limestone beds of the Morro Formation dip almost vertically and are thrust towards the NE (Mte Branco Thrust; Fig. 2b). Other outcrop locations are heavily intruded by dykes or covered by alluvium.

The Morro Formation consists of up to ~ 3 dm-thick beds of grey limestones that contain cm-sized chert lenses and bands, and show fine and swirly lamination. Stylolites are common and bioturbation is observed in the form of burrows, up to 2 cm in diameter and often associated with diagenetic dolomite rhombs (Appendix C). Thin sections of the Morro Formation rocks reveal radiolaria (in the form of calcite-filled solution-molds), and rare fragments of gastropods, sponge spicules, echinoid fragments, radiolaria (*Nasselaria*) and foraminifera. At Mte Esgrovere, we found ammonites and aptychi, ~ 150 m above the stratigraphic base of the Morro Formation (Latitude/Longitude: 15.162936, − 23.182217). Some of these ammonites are well preserved and were identified as *Phylloceras* cf. *infundibulum* (d'Orbigny 1840) and *Neocomites neocomiensis* (d'Orbigny 1841) (Appendix C), which indicates a Valanginian to early Hauterivian age (136.4–130 Ma; Fossilworks.org 2019) and supports similar ammonite findings at Mte Esgrovere by Casson et al. (2020). At Rib do Morro, we also found ammonites exposed on a bedding surface ~ 140 m above the Morro Formation stratigraphic base. These ammonites are unfortunately not well preserved, but confirm the first descriptions of ammonites from this location by Stahlecker (1934) that were revised by Casson et al. (2020). Additionally, the Morro Formation rocks contain Early Cretaceous nannofossils of biostratigraphic value (listed in Appendix C), which support Valanginian to Early Aptian ages as quoted by Casson et al. (2020).

The Carqueijo Formation overlies the Morro Formation rocks and consists of cm-thick limestone beds, alternating with cm-thick elongated chert bands (usually 2–3 cm thick, locally up to 10 cm thick), soft marls, and marly and shaley limestones. Bright purple and green coloration of these rocks suggest hydrothermal alteration, which is commonly observed, as well as the occurrence of dyke intrusions. Macrofossils are rare, but thin sections reveal abundant calcite filled solution molds of radiolaria, and some samples yield nannofossils of biostratigraphic value (listed in Appendix C).

The Coruja Formation successions contain tuffs and conglomerates, which overlay the Carqueijo Formation and were mapped for large areas in the N and NW of the Basement Complex, and W of Mte Penoso (Serralheiro 1970; Stillman et al. 1982). However, we found that especially flat areas are covered by Quaternerary sediments, plus reforestation and deposition of recent sediments cover many of the originally described outcrop locations. We were able to confirm the occurrence of Coruja Formation outcrops at the southern foot of Mte Penoso, and at the SW flank of Lombo Vermelho, where the formation is composed of orange weathered tuffs, bioturbated sandstones, and conglomerates (Appendix C). The conglomerates contain wavy-cross-bedding and channel structures. Conglomerate clasts are strongly altered, and the original mineralogy was replaced by secondary minerals, despite partly retaining the original igneous textures. Unfortunately, these clasts were too altered to be used for ^{40}Ar–^{39}Ar dating.

Miocene deposits

The Early Miocene CIC is exposed in the southern central part of Maio island, where it forms a relatively flat, almost bowl-shaped, topography (Figs. 1, 2). It is composed of intrusions of essexites, syenites, and pyroxenites, cut by numerous basanitic, ankaramitic, trachytic, and carbonatite dykes. These Miocene units intruded the Early Cretaceous pillow lavas of the Batalha Formation, and the Early Cretaceous pelagic limestones of the Morro and Carqueijo Formations, which were uplifted and partly tilted during magmatic intrusion activity. The rocks of the Basement Complex are also discordantly overlain by Miocene volcanic deposits. The Casas Velhas Formation, composed of ankaramite lava flows, is exposed in river sections in the S and SW of Maio (Fig. 1). In the NE of Maio, the sediment-dominated Pedro Vaz Formation is exposed (Fig. 1), and is typically composed of conglomerates that contain (sub-) rounded igneous clasts, with clast diameters of up to 40 cm. Locally, pyroclastic deposits (tuffs and ignimbrites) and ankaramite lavas appear as lenticular bodies in sections within this formation. This agrees well with observations of Stillman et al. (1982),

suggesting that the Pedro Vaz Formation crops out mainly between the Mte Penoso and Mte Santo António.

In the W and SE of Maio, the olivine-nephelinites and melilitites of the Malhada Pedra Formation are exposed (Fig. 1). These rocks are thickest at Mte Batalha and inclined to the SE. In the NE of Mte Esgrovere, these rocks are exposed in an open pit mine, where they form columns. Along the road towards Figueira da Horta, pillow lavas are also exposed, suggesting partial formation during periods of sea-level highstands.

The youngest volcanic rocks on Maio belong to the Mte Penoso Formation, which is exposed on Mte Penoso and Mte Santo António in the N of Maio (Fig. 1). Ankaramite lava flows are interbedded with tuffs and other pyroclastic deposits. The Mte Penoso Formation once formed a stratovolcano, with units dipping towards the NE (Stillman et al. 1982). The Mte Penoso Formation rests unconformably on rocks of the Coruja Formation at the southern flanks of Mte Penoso and Lombo Vermelho (Fig. 2c), and on conglomerates and pyroclastics of the Pedro Vaz Formation. Feeder dykes to the former stratovolcano are observed in the northern part of the island, where they cross-cut underlying rock units.

All formations on Maio are cross-cut by dykes, especially in the older parts of the island, where the dyke density is very high and obscures former rock units. Carbonatite dykes are present, especially in the pelagic limestones and intrusive rocks of the CIC. A larger complex of carbonatites is present E of Mte Vermelho and NW of Mte Penoso (Fig. 1).

^{40}Ar–^{39}Ar ages of dykes and tectonic structures in the Basement Complex

A small area of Batalha Formation rocks is exposed at the NE flank of Mte Branco (Figs. 2b, 4). At this location, the shape of the pillows is still visible, but they were heavily intruded by dykes (Fig. 4a). These dykes are all truncated by the Mte Branco Thrust (Fig. 4b, c), and faults and fractures parallel to this thrust were subsequently filled with calcite.

We obtained 100 structural measurements (dip direction/dip) of dykes intruding the Batalha Formation (Fig. 4d–f; Appendix D). Dip angles vary between 25° and 90°. One third of the measured dykes are almost vertical with dip angles of > 80°, and the majority (60%) have dip angles between 50° and 79° (Fig. 4). The steep dykes (> 80°) dip towards the NW, NNE and SSE (Fig. 4d, f). The moderately dipping dykes (25–79°) have a larger variation in orientations, but also show a similar NW dipping component (Fig. 4d, e). However, there is also an additional group of ENE and E dipping dykes, and a minor SSE dipping component (Fig. 4d, e). Dykes dipping towards the SW are completely absent (Fig. 4d). In two cases, the age relationships of the dykes were recorded by cross-cutting relationships. The older dykes are inclined towards the W and NW (275/58 and 341/63), while the younger dykes cross-cut the old dykes and dip towards the NE (053/53 and 044/59).

Two nephelinite dykes were sampled from the Batalha Formation (Table 1). Sample 17–73 yields a phlogopite ^{40}Ar–^{39}Ar single-crystal total-fusion weighted mean age of 10.570 ± 0.053 Ma (Mean Square of Deviation (MSWD) = 1.49, Probability (P) = 8%, n = 20, excluding the 4 youngest ages (8.95–9.61 Ma) that contained some of the highest ^{36}Ar/^{39}Ar AI values, which may indicate some radiogenic ^{40}Ar (^{40}Ar*) loss; Table 2; Appendix B). Sample 17–74 yields a phlogopite ^{40}Ar–^{39}Ar single-crystal total-fusion weighted mean age of 10.405 ± 0.033 Ma (MSWD = 1.12, P = 32%, n = 22, excluding the 2 youngest ages (9.70 and 10.15 Ma) that may have suffered some ^{40}Ar* loss; Table 2; Appendix B). Multi-grain step-heating of these two phlogopite samples yields disturbed staircase-rising age spectra, which suggest possible ^{40}Ar* loss as a result of alteration. However, the high-temperature step ages of 10.466 ± 0.070 Ma (29.9% ^{39}Ar, MSWD = 1.94, P = 7%; sample 17–74) and 10.61 ± 0.13 Ma (18.7% ^{39}Ar, MSWD = 4.39, P = 0%; sample 17–73) are within 2σ errors of the single-crystal total-fusion ages (Table 2; Appendix B).

At the SW flank of Mte Branco, above the Mte Branco Thrust, the dm-thick banks of massive pelagic limestones from the Cretaceous Morro Formation were intruded by alkaline dykes (Fig. 4g). These dykes dip with angles of 10° to 24° towards the N with undulating orientations (dip direction/dip: 336/10, 007/24, 358/21), and show an angle of ~ 45° to the bedding of the Morro Formation that dips towards the NE. In contrast, the dykes that intruded the underlying Batalha Formation are mostly steeper dipping (25° to 90°). Two phlogopite grain fractions from one nosean nephelinite dyke sample (17–16/3) in the Morro Formation (Fig. 4h; Table 1) were dated by the single-crystal total-fusion ^{40}Ar–^{39}Ar technique, yielding 2σ-error overlapping ages of 9.292 ± 0.028 Ma (0.25–0.5 mm, MSWD = 1.31, P = 15%, n = 24), and 9.268 ± 0.028 Ma (0.5–1 mm, MSWD = 0.88, P = 62%, n = 23; Table 2). Combining the data from both phlogopite size fractions yields a ^{40}Ar–^{39}Ar single-crystal total-fusion weighted mean age of 9.282 ± 0.022 Ma (MSWD = 1.13, P = 26%, n = 47), which is within 2σ errors of the multi-grain step-heating plateau age of 9.263 ± 0.024 Ma (0.25–0.5 mm fraction, MSWD = 1.22, P = 23%, 100% ^{39}Ar; Table 2; Appendix B). Thus, a combined ^{40}Ar*/^{39}Ar single-crystal total-fusion and step-heating age of 9.273 ± 0.020 Ma (MSWD = 1.17, P = 16%, n = 67) was calculated, using the approach of Heath et al. (2018) for sample 17-16/3.

Miocene mass wasting deposit and its ^{40}Ar–^{39}Ar age

At the base of Mte Penoso and at the southern flank of Lombo Vermelho, conglomerates are found that had not previously been described in detail (Figs. 2c, 5). The two

main outcrop areas are separated by more than 1 km across an erosional valley. Below Mte Penoso, exposed to the W and S, this ~ 50 m-thick conglomerate sequence is exposed from ~ 200 m a.s.l. in the valley to ~ 250 m asl and was laterally traced for ~ 1 km along the base of the hill. It is overlain by lava flows and pyroclastic deposits of the Mte Penoso Formation (Fig. 5a). The conglomerate is polymict and poorly sorted, with clasts typically ranging from centimetres to several decimetres in diameter. Clast sizes vary by more than one order of magnitude at any location. The clast contents range between ~ 25 and 50 volume %, resulting in both matrix-supported and clast-supported fabrics on an outcrop scale (Fig. 5b-d). Some areas comprise subunits or flow units identified by difference in dominant grain size, typically separated by a thin indistinct transition zone. The individual clasts range from angular through sub-angular and sub-rounded to well rounded and are set in a weathered matrix that locally shows signs of hydrothermal alteration. Similar sequences have been characterized as debris flow or flank collapse deposits (e.g., Nemec and Steel 1984). The clasts represent a wide range of rock fragments, including alkali-basaltic and nephelinitic fragments ranging from dense to vesicle-rich, ankaramite, phonolite lava, and subordinate alkaline plutonic fragments, which closely resemble the Miocene igneous rocks on Maio. Many clasts are weathered and some show possible hydrothermal alteration. Locally, pyroclastic, lenticular units and occasional small lava flows are also identified and the deposit is therefore multi-phase, testifying to intermittent volcanism during this erosional period.

At Lombo Vermelho, such conglomerates also crop out discordantly above units of the Carqueijo and Coruja Formations, which were in turn intruded by numerous dykes. The Lombo Vermelho conglomerate is also overlain by lava flows and pyroclastic deposits of the Mte Penoso Formation (Fig. 5e), but at this location the conglomerates are thinner (~ 20 to 30 m thick) compared to the Mte Penoso outcrop area (~ 50 m thick). Clasts have been derived from various lithologies as described above for Mte Penoso, but additionally include subordinate limestone and sedimentary rocks from the underlying Carqueijo Formation. The lower part of this conglomerate was strongly hydrothermally altered and shows a network of secondary mineralized cracks.

To ^{40}Ar–^{39}Ar date this unit, fresh phlogopites of 0.25–0.5 mm and 0.5–1 mm grain sizes were separated from a slightly altered nosean nephelinite clast (sample 18-32/3; Table 1), collected below the base of Mte Penoso. This clast yields ^{40}Ar–^{39}Ar ages ranging from 8.51 ± 0.12 Ma to 11.75 ± 0.34 Ma for both size fractions, with 2σ-error overlapping weighted mean ages of 8.707 ± 0.045 Ma (MSWD = 1.18, P = 30%, n = 11) and 8.654 ± 0.029 Ma (MSWD—1.42, P = 12%, n = 18) for the 0.25–0.5 mm and 0.5–1 mm size fractions, respectively. This broad range of ages in both size fractions may be explained by the presence of different generations of antecrysts or xenocrysts. Based on their weight % (wt%) K contents and ^{40}Ar–^{39}Ar ages, three different groups of phlogopites were identified from the two combined size fraction data: (1) the youngest group of 29 phlogopites yielded a weighted mean age of 8.666 ± 0.027 Ma (MSWD = 1.48, P = 5%, n = 29) with high wt% K (5.6–7.9) and % ^{40}Ar* (73–95) contents; (2) a slightly older group of three phlogopite grains that yielded a weighted mean age of 8.825 ± 0.062 Ma (MSWD = 0.19, P = 83%, n = 3) with high wt% K (5.5–6.3) and % ^{40}Ar* (79–93) contents; and (3) the oldest group of four phlogopites (9.68 ± 0.13 to 11.75 ± 0.34 Ma) that contained low wt% K (3.0–4.5) and % ^{40}Ar* (54–78) contents (Table 2). The Group 1 (8.666 ± 0.027 Ma) phlogopites were interpreted as being phenocrysts, whilst the Group 2 (8.825 ± 0.062 Ma) phlogopites were possibly antecrysts or xenocrysts from an older local magma that were picked up during ascent of the erupted younger magma. The low wt% K contents in the older Group 3 (9.68 ± 0.13 to 11.75 ± 0.34 Ma) phlogopites may indicate the presence of composite grains (i.e., phlogopite crystals finely interlayered with a low-K mineral) that can result in anomalous ^{40}Ar–^{39}Ar ages due to ^{39}Ar recoil effects (Di Vincenzo et al. 2003). Alternatively, the four older phlogopite grains may have been xeno-/antecrysts that suffered some weathering or hydrothermal alteration, resulting in some K and ^{40}Ar* loss and disturbed ^{40}Ar–^{39}Ar ages.

Discussion

Age of intrusive growth, dyke emplacement and tectonic activity at Mte Branco

Two of our nephelinite dyke samples were found intruding Batalha Formation rocks below the Mte Branco Thrust (Fig. 4), yielding ^{40}Ar–^{39}Ar ages of 10.570 ± 0.053 Ma and 10.405 ± 0.033 Ma (Table 2). On the southern coast of Maio, dykes intruding the Batalha Formation yield various K–Ar ages ranging from 12.2 to 9.1 Ma (12.2 ± 0.4 Ma, 11.1 ± 0.6 Ma, 10.8 ± 0.4 Ma and 9.1 ± 0.4 Ma; Mitchell et al. 1983), which partly overlap with our ^{40}Ar–^{39}Ar ages for the Monte Branco area further north (Fig. 6). Our new ^{40}Ar–^{39}Ar phlogopite ages overlap within 2σ errors with 2 of the 3 literature K–Ar ages (11.0 ± 0.6 Ma, 10.8 ± 2.2 Ma and 9.9 ± 0.4 Ma) from alkaline lamprophyre dykes cutting the nearby Albian Carqueijo Formation (Mitchell et al. 1983) and 2 of the youngest K–Ar ages from dyke intrusions in the CIC (10.9 ± 0.8 Ma to 10.0 ± 0.8 Ma; Fig. 6). In addition, they overlap within 2σ errors with

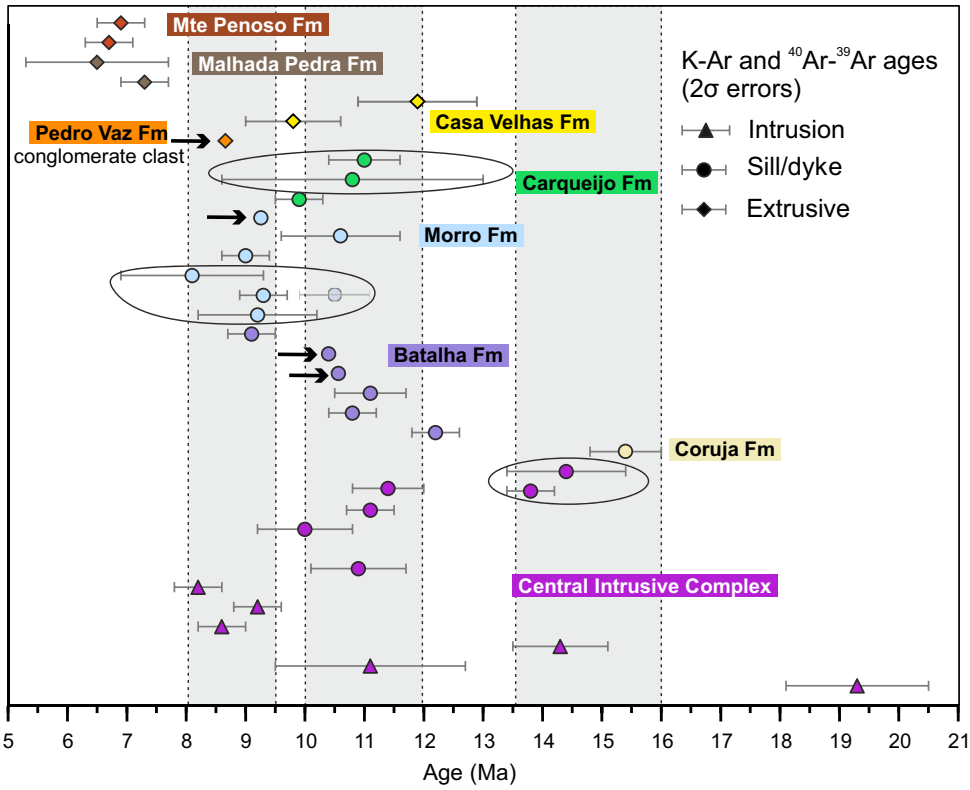

Fig. 6 Compilation of available Miocene K–Ar and ^{40}Ar–^{39}Ar ages (all with 2σ errors) from Maio, Cabo Verde (Bernard-Griffiths et al. 1975; Mitchell et al. 1983; Ramalho 2011), including new ^{40}Ar–^{39}Ar ages presented in this study (marked by black arrows). The colors of the data points are based on the colors of the rock formations in the geological map (Fig. 1). Grey shaded areas indicate suggested phases of volcanic activity. Data that originated from one sample but yielded different K–Ar or ^{40}Ar–^{39}Ar ages are encircled. The small 2σ errors for our new ^{40}Ar–^{39}Ar ages are smaller than the symbol sizes

a K–Ar age from a Casas Velhas Formation ankaramite lava (9.8 ± 0.8 Ma; Mitchell et al. 1983).

The preferred ^{40}Ar–^{39}Ar age of 9.273 ± 0.020 Ma for our Morro Formation dyke sample from the Mte Branco region overlaps within 2σ errors with all 4 K–Ar ages (9.3 ± 0.4 to 8.1 ± 1.2 Ma) obtained from two samples of Mte Branco basanite and ankaramite intrusions presented by Mitchell et al. (1983; Fig. 6). However, Mitchell et al. (1983) obtained an older ^{40}Ar–^{39}Ar plateau age (10.5 ± 0.6 Ma) from a split of the same Morro Formation/Mte Branco basanite sill that also yielded younger 3 K–Ar sample split ages of 9.3 ± 0.5 to 8.1 ± 1.2 Ma. This 10.5 Ma older age is similar to a Bernard-Griffiths et al. (1975) K–Ar age of 10.6 ± 1.0 Ma for micas from a carbonatite dyke sample at Mte Branco (Fig. 6). Mitchell et al. (1983) suggest that the formation age of their basanite sill is 10.5 Ma and their three younger K–Ar ages may have been reset by a younger event, even though their samples are fresh and show no evidence of thermal overprinting. It is difficult to confirm the Mitchell et al. (1983) 10.5 ± 0.6 Ma ^{40}Ar–^{39}Ar age, as no accompanying isochron or inverse isochron data are presented to confirm this plateau age. Given the very fresh nature of the phlogopites from our Morro Formation nosean nephelinite dyke sample and reproducible ^{40}Ar–^{39}Ar single-crystal total-fusion and inverse isochron ages, we are confident that the 9.273 ± 0.020 Ma is a magmatic formation age.

The context of multiple phases of intrusive growth is verified by the new and published geochronology ages. The overall distribution of new and published dyke K–Ar and ^{40}Ar–^{39}Ar ages suggest the preservation of several phases of intrusive growth in the different rock formations of Maio (Fig. 6; Grunau et al. 1975; Bernard-Griffiths et al. 1975; Mitchell et al. 1983; Ramalho 2011). Gabbros, essexites, pyroxenites and syenites from the CIC yield K–Ar ages of 8.2 ± 0.4 up to 21.6 ± 12.6 Ma (Grunau et al. 1975; Mitchell et al. 1983). However, the 2σ errors are large for some of these ages, therefore we chose to reject the three Grunau et al. (1975) K–Ar ages with the largest 2σ errors of 12.5 ± 4.8 Ma, 14.0 ± 8.0 Ma and 21.6 ± 12.6 Ma, as these cannot be used for any time discrimination in such a young age interval. Based on the combined ^{40}Ar–^{39}Ar and K–Ar age data of dyke and sill intrusions we tentatively suggest different periods of intense intrusive activity and by inference correspondingly high volcanic activity in Maio: (1) a first phase from ~ 16 to 13.5 Ma is recorded in dykes that intrude CIC and Coruja Formation rocks; (2) a second phase from ~ 12 to 10 Ma is obtained primarily in dykes that intruded the CIC, Batalha and Carqueijo Formations; and (3) a final phase from ~ 9.5 to 8 Ma is recorded mainly in dykes that intrude Morro Formation rocks (Fig. 6). We emphasise that the second and third phases partly overlap in time, but represent a geographical shift in dyking and intrusion activity. All three phases are recorded in dykes/sills and overlap

within 2σ errors with the K–Ar and ^{40}Ar–^{39}Ar ages recorded in the CIC intrusive rocks (Fig. 6). The second (~ 12–10 Ma) phase is previously mentioned by Mitchell et al. (1983) as a period of intense intrusive activity on Maio. It is interesting to note that this ~ 12–10 Ma phase mainly records dyke/sill emplacement in the CIC, Batalha, and Carqueijo Formations, whereas the third phase (~ 9.5–8 Ma) is mainly recorded in dykes that intrude Morro Formation rocks in the Mte Branco area. The different geographical and lithological distributions of ages could be explained by a geographical shift in volcanic activity or be caused by tectonic activity. Both the second and third phases overlap with K–Ar and ^{40}Ar–^{39}Ar ages of ankaramite lavas from the Casas Velhas Formation (11.9 ± 1.0 Ma and 9.8 ± 0.8 Ma; Mitchell et al. 1983; Ramalho 2011).

At one of our study locations, N of Mte Branco, the pillow lavas are intensely intruded by numerous dykes that are all truncated by the Mte Branco Thrust. The variation in dip angles from vertical to 25° suggests different groups of intrusions, varying from steep dykes to inclined sheets. The dip directions of the moderately dipping dykes (25° to 79°) suggest conjugate extension (dipping twoards NW and ESE; Fig. 4d, e), which may be due to a doming process caused by magmatic underplating and thermal uplift (e.g., Klügel et al. 2005). However, we cannot exclude the possibility that the orientations of the Batalha Formation rocks were also changed due to tectonic activity.

In general, the dykes that intruded the Morro Formation are younger than the Batalha Formation dykes below the Mte Branco Thrust and they also show different orientations: while the dykes in the Morro Formation dip towards the North and are relatively flat (336/10, 007/24 and 358/21), the dykes in the Batalha Formation below the thrust show various orientations (NW, ENE and SSE for the moderately dipping dykes and NW, NNE and SSE for the almost vertical dykes) The different orientations of dykes suggest different pulses of magma and therefore different phases of intrusive activity, which could be related to various growth stages in the CIC. However, the dyke orientations may have changed due to the thrusting and tectonic activity and, therefore, cannot be used to establish former eruption centres.

Miocene erosive activity: conglomerates

The conglomerates at the base of Mte Penoso and at the southern flank of Lombo Vermelho are variable in composition, rounding and grain sizes of clasts, and in facies types. This variability is typical for complex volcanic landslide and debris avalanche deposits (e.g., Bernard et al. 2009; Roverato et al. 2014; van Wyk de Vries and Delcamp 2015). In general, overloading, over-steepening, uplift and subsidence, magma emplacement in the crust and erosion can destabilize a volcanic edifice. Furthermore, debris avalanches and flank collapse events may be triggered by magmatic (intrusive or extrusive), seismogenic (tectonic/volcanic earthquakes), or environmental (sea level changes, precipitation) events (McGuire 1996).

According to Serralheiro (1970) and Stillman et al. (1982), the Pedro Vaz Formation crops out mainly between Mte Penoso and Mte Santo António and in small patches in the SW of Maio (e.g., Rib do Morro, close to Barreiro; Fig. 1). It contains "rudites" or matrix-supported conglomerates, interbedded with fine "tuffs" and ankaramite lava flows, separated by thin "arenites", and is intruded by numerous ankaramite dykes (Stillman et al. 1982). Locally confined, it apparently includes material from the underlying Casas Velhas Formation (Stillman et al. 1982). The deposits presented in this study are mainly composed of polymict conglomerates and contain dispersed pyroclastic rocks and lava flows, which agrees well with the descriptions of Stillman et al. (1982). Based on their stratigraphic position and the resemblance to previous descriptions, we therefore suggest that the conglomerates presented in our study are part of the Pedro Vaz Formation. An overlap in ages between the Pedro Vaz and Casas Velhas Formations is also noted by Casson et al. (2020; Fig. 3).

The Pedro Vaz Formation multi-phase deposits represent a period of both rapid erosion (landslides and flank collapses) and simultaneous moderate volcanic growth (pyroclastic flows and lavas), which most likely coincides with the onset of rejuvenated magmatic activity. Such periods of simultaneous volcano growth and destruction are common worldwide (e.g., Tutucapa volcano, Peru (Valderrama Murillo 2016); Stromboli, Italy (Romagnoli et al. 2009); Mount St. Helens, USA (McEwen and Malin 1989); Augustine volcano, Alaska (Begét and Kienle 1992); Tenerife, Canary Islands (Hunt et al. 2011, 2013, 2018); and Montserrat (Cassidy et al. 2014)). The shield stage of an ocean island volcano is defined as the period with highest magma supply rates and thus the most rapid growth. Intense erosion processes dominate the morphologic evolution of the mature edifice, as magma extrusion and intrusion rates diminish towards the end of the shield stage (Carracedo 1999; Ramalho et al. 2013). Such erosional phases are well-documented worldwide and include gravity sliding on both local and regional scales (e.g., Hunt et al. 2018; Urlaub et al. 2018). For example, in the Cabo Verde Archipelago, several large landslides and flank collapses have been described (Day et al. 1999; Le Bas et al. 2007; Masson et al. 2008; Ancochea et al. 2010; Martínez-Moreno et al. 2018; Barrett et al. 2020). Land slide deposits on São Vicente can also be compared to the conglomerates on Maio (Ancochea et al. 2010).

Our new 8.7 Ma ^{40}Ar–^{39}Ar age data combined with literature K–Ar and ^{40}Ar–^{39}Ar ages of the overlying Malhada Pedra and Monte Penoso Formations (Bernard-Griffiths et al. 1975; Mitchell et al. 1983) confine the Miocene erosional phase at Maio to between 8.7 and 6.7 Ma (base of

Monte Penoso Formation), coinciding with dispersed and rejuvenated volcanism of the temporally overlapping Malhada Pedra and Pedro Vaz Formations. We additionally suggest that flank collapse activity and rapid mass wasting in the Tortonain/Messinian (8.7–6.7 Ma) may have enhanced the rejuvenated igneous activity on Maio, due to decompression-induced melting at upper mantle depths (Manconi et al. 2009; Cassidy et al. 2015; Hunt et al. 2018). It remains unclear what caused the presented multiphase flank collapse events. They may have been emplaced contemporaneously with fault activity along the Mte Branco Thrust, which was possibly active between 9 and 8.7 Ma, following the final dyke intrusions at Mte Branco. However, the collapse events could also have been influenced by early rejuvenated activity of Malhada Pedra and/or Monte Penoso Formations, which may have formed the local pyroclastic sequences within the conglomerate sequences.

The well-constrained ^{40}Ar–^{39}Ar phlogopite age of 8.666 ± 0.027 Ma obtained from a nosean nephelinite clast within the conglomerate directly underlying the Mte Penoso Formation is regarded as a maximum age for this conglomerate deposit and a minimum age for previous igneous units (i.e., the Casas Velhas Formation). The presence of two older age groups of phlogopites within this sample may indicate the presence of older phlogopite antecrysts and/or xenocrysts, which are distinguished by their ages and wt.% K contents (Table 2; Appendix B). Xeno-/antecrysts in igneous rocks are typical for Cabo Verde rocks and the plumbing system below the islands and seamounts (e.g., Samrock et al. 2019; Barker et al. 2019, 2021) and is further supported by the presence of rounded phlogopites in the sample (Appendix A).

Refined geological model of Maio

Based on field observations and new ^{40}Ar–^{39}Ar dating of dykes and a conglomerate clast, we present a refined model of the geological evolution of Maio (Fig. 7).

Initially, Early Cretaceous pillow lavas of the Batalha Formation and Early Cretaceous pelagic limestones from the Morro and Carqueijo Formations are deposited on the sea floor (Fig. 7a; e.g., Robertson 1984, Casson et al. 2020). We confirm descriptions of red intercalated sediments that include calpionellids in the upper Batalha Formation at Mte Esgrovere (Fourcade et al. 1990; Casson et al. 2020). Our ammonite findings and microfossil assemblages in the Morro Formation matches the previously proposed Valanginian to Early Aptian ages for the Morro Formation and the Albian age for the overlying Carqueijo Formation (Casson et al. 2020).

It is unclear when subaerial volcanism on Maio started, as there are little data for the rare outcrops of the Coruja Formation. Mitchell et al. (1983) published K–Ar ages for Coruja Formation igneous clasts in a conglomerate, yielding Late Jurassic to Late Cretaceous ages (157.8 ± 8.0, 99.8 ± 4.4, and 73.2 ± 2.4 Ma). Rare planktonic foraminifera suggest a Paleocene to Early Miocene age for the Coruja Formation, but the precise age of these units, and therefore the age of the first subaerial volcanism on Maio, remains weakly constrained (Robertson 1984). Gravity data suggest that an eruptive center is located in the SE of Maio (Represas et al. 2012). In this area, dyke density is high and rocks of the Miocene CIC are mainly preserved, and most successions of sedimentary units of the Basement Complex have been removed by erosion. However, early volcanic units are absent; therefore, it is not clear if there is an early volcanic center in SE Maio. Volcanic ash layers in marine sediments NE of the Cabo Verde Archipelago suggest the onset of volcanism on the Cabo Verde Islands during the early Middle Miocene (DSDP Site 368; Lancelot et al. 1978).

During the Early Miocene (at or before 19.3 ± 1.2 Ma; Mitchell et al. 1983) the CIC begins to form with the emplacement of shallow intrusions in the middle and upper crust, i.e., the formation of an intrusive core complex (Fig. 7b, c). Such pronounced intrusion activity is typically associated with volcanic activity and we also assume this in this case for Maio. Emplacement of plutonic rocks led to mechanical and thermal uplift and doming, which induced the semi-circular dip of the former seafloor units (Fig. 7b; Serralheiro 1970), and stoping probably led to the disruption of strata above the intrusive complex (e.g., Klügel et al. 2005, 2015; Montanari et al. 2017).This intrusive period may have lasted only a few million years, leading to a rapid flare up and accompanying uplift of the edifice (Klügel et al. 2005). Such comparatively rapid uplift has also been recorded from other Cabo Verde islands, e.g., Santiago (Marques et al. 2020). It has been shown that locally confined intrusive activity at crustal levels is responsible for distinct island uplift in the region (Ramalho et al. 2010b, c; Ramalho 2011). The intrusive activity also caused crustal thickening, with the thickest crust being present below the older eastern islands of the Cabo Verde Archipelago, such as Sal and Maio (Lodge and Helffrich 2006).

At a later stage of intrusive island growth (from ~ 12 to 8 Ma; Fig.7d, e), dyke emplacement plays a more important role. Some dykes probably stalled, leading to edifice growth at depth, while others reached the surface, feeding eruptions and extrusive growth and emplacement of the Casas Velhas Formation. The importance of dyke emplacement to the growth of volcanic edifices has been shown previously (e.g., Annen et al. 2001; Kervyn et al. 2009). The Casas Velhas Formation may be regarded as rocks from a 'Lower Volcanic Complex' and is possibly associated with a shield building stage, which may have started prior to ~ 11.9 Ma and overlaps with the last intrusive activity in the CIC that phased out at ~ 8 Ma (Fig. 7d, e; Ramalho 2011). The three high activity intrusive phases recorded in dykes (16–13.5 Ma, 12–10 Ma, and 9.5–8 Ma; Fig. 6) overlap with ages recorded in intrusive rocks from the

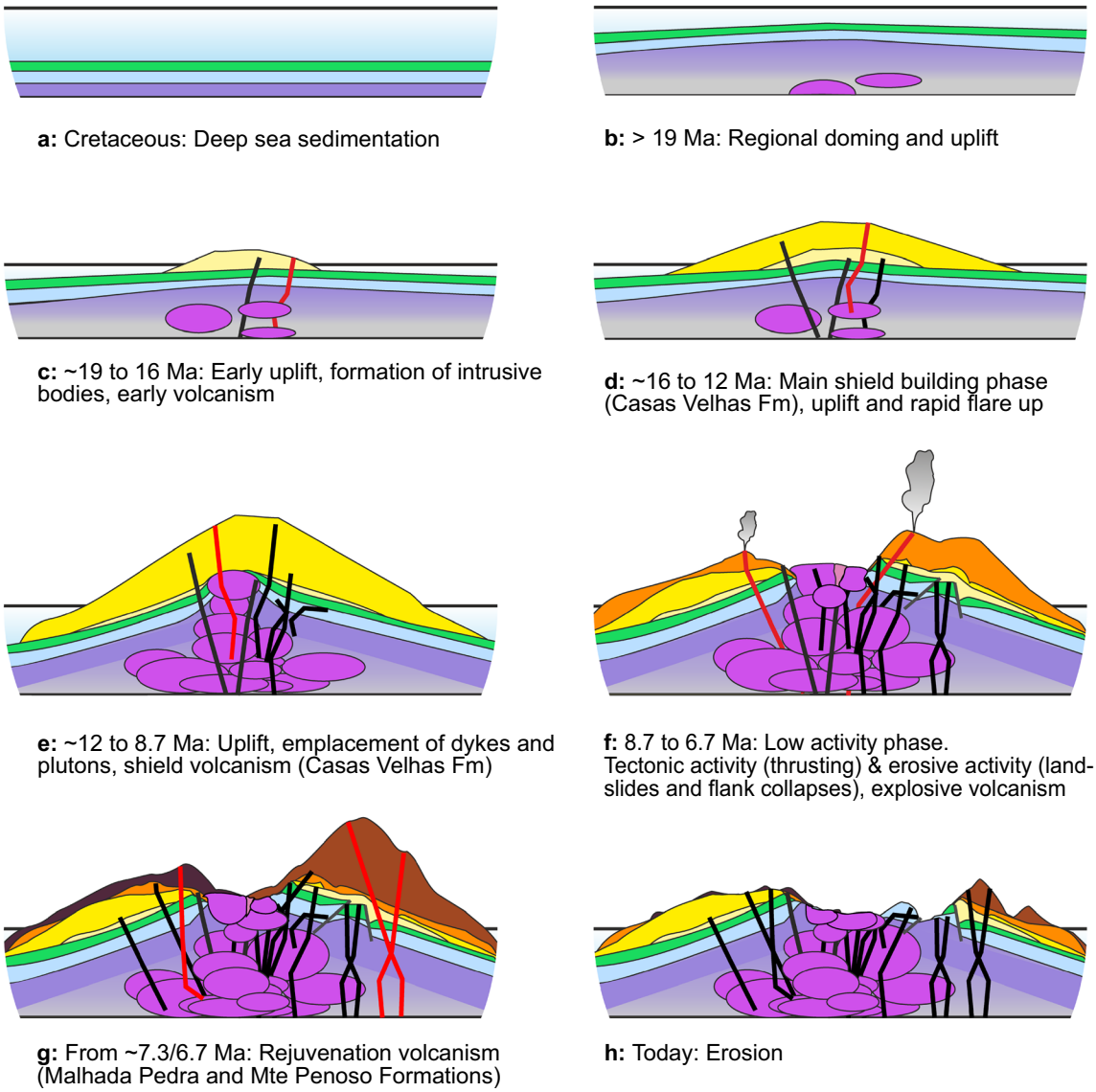

Fig. 7 Cartoon of a simplified Maio geological evolution model (**a**–**h**; not drawn to scale and omitting sea level changes). Red lines = active dykes, black lines = cooled dykes

CIC, which may partly be due to the overprinting of older rocks (Bernard-Griffiths et al. 1975; Mitchell et al. 1983).

Intrusive activity not only led to edifice growth from the inside, but also to extrusive activity and growth on the outside. Dyke K–Ar and ^{40}Ar–^{39}Ar ages from the second and third intrusive phases (12–10 Ma and 9.5–8 Ma) correspond with K–Ar ages from the subaerial Casas Velhas Formation lava flows and pyroclastic rocks, which are preserved in the S and SW parts of the island, mainly in river sections (Mitchell et al. 1983; Fig. 1). Casas Velhas Formation rocks are not preserved in the N and NE parts of Maio, possibly due to the later flank collapse events, but dykes of similar ages are present in these regions. An ankaramite lava from the base of the Casas Velhas Formation in the S of Maio yields a K–Ar age of 9.8 ± 0.4 Ma (Mitchell et al. 1983), although the authors suggest that the age may be older as the dyke may have been thermally overprinted due to the high dyke density at the sampling location. Mitchell et al. (1983) additionally observed petrological similarities between the youngest group of plutonic rocks from the CIC in the NW of Maio (Mte Vermelho) and lavas from the Casas Velhas Formation. This suggests that parts of the CIC and dykes cutting the Basement Complex rocks are the intrusive counterpart of the extrusive volcanics in the Casas Velhas Formation, with some of the dykes feeding surface eruptions. The ^{40}Ar–^{39}Ar age of 8.666 ± 0.027 Ma for a conglomerate clast from the Pedro Vaz Formation additionally overlaps with CIC and Casas Velhas Formation ages, further constraining igneous activity during the Tortonian.

A period of strong erosion and low volcanic activity followed the deposition of the Casas Velhas Formation lava flows, as shown by the emplacement of massive conglomerates and sparse pyroclastic deposits and the removal of large volumes of the previous volcanic edifice (Figs. 2c, 3, 7f). The 8.666 ± 0.027 Ma ^{40}Ar–^{39}Ar phlogopite age from a nephelinite clast from the Pedro Vaz Formation conglomerate, and the 6.7 ± 0.4 Ma K–Ar age from an ankaramite from the base of Mte Penoso (Mitchell et al. 1983), can be used to confine this erosive period to the Tortonian/Messinian. The sediment-dominated Pedro Vaz Formation is described as locally overlying the volcanic-dominated Casa Velhas Formation and incorporated rocks from the Casas Velhas Formation rocks in its base (i.e., in the western part of Rib do Morro and N of Barreiro; Serralheiro 1970; Stillman et al. 1982). Similar sedimentary deposits, which are locally confined and heterogenous, are difficult to differentiate and therefore it is hard to constrain their relative ages. This is especially true in this sequence of laterally heterogeneous units. We suggest that the younger parts of both the volcanic-dominated Casas Velhas Formation in the SW and the sediment-dominated Pedro Vaz Formation in the NE show similar features (i.e., conglomerates with pyroclastic layers) and they may overlap in age.

Previously published ages of the Pedro Vaz Formation are based on foraminifera findings from siltstones collected in the Pedro Vaz area (Rigassi 1972), who suggested an open sea environment and a planktonic zone N12 of Middle Miocene age. Reexamination of the Rigassi (1972) list of foraminifera reveals that only *Globorotalia fohsi robusta* and *G. fohsi lobata* are currently relevant for biostratigraphy and are now listed as modifications of *Fohsella fohsi* (s.l.) (J. Schönfeld, pers. comm.; Wade et al. 2011). This supports planktonic zone N12 (reclassified as M9a–M9b) with ages of 13.41–11.79 Ma (Wade et al. 2011). The Rigassi (1972) Pedro Vaz Formation microfossils have been previously used to confirm Miocene (> 12 Ma) ages for the underlying Casas Velhas Formation. However, Stillman et al. (1982) states that the intercalation of open-sea rocks with subaerial lavas and conglomerates is problematic and thus these interpretations should be treated with caution.

Tectonic activity on the Mte Branco Thrust must postdate the intrusive activity in the Batalha Formation, as the dykes are all truncated by the thrust, which must therefore be younger than 10.405 ± 0.033 Ma. It is not clear if one of the Mitchell et al. (1983) samples from Mte Branco, yielding a K–Ar age of 9.0 ± 0.4 Ma, comes from the hanging or the foot wall of the thrust, but Mitchell et al. (1983) mention that it is truncated by the thrust, therefore the age of this thrust must also be younger than 9.0 Ma. Such reverse faults are common in volcanic settings around the world and typically occur at the end of the doming process caused by shallow magmatic intrusions (Montanari et al. 2017). Tectonic activity may have triggered the major Late Miocene erosive events, thus leading to the formation of sedimentary deposits overlying the Basement Complex Rocks (below Mte Penoso, in the Pedro Vaz Formation) and may therefore be contemporaneous in age (Tortonian/Messinian; Fig. 7f).

The eruption of Malhada Pedra Formation rocks (olivine melilitites) and Mte Penoso Formation nephelinite lavas mark the final phase of volcanism (Fig. 7g). Both formations are physically separated due to the deep erosion levels in the central part of Maio, but have overlapping ages: The Malhada Pedra olivine melilitite lavas yield K–Ar ages of 7.3 ± 0.4 Ma and 6.5 ± 1.2 Ma, whereas ankaramites from the base of the Mte Penoso lava pile and from Mte Santo António give K–Ar ages of 6.7 ± 0.4, and 6.9 ± 0.4 Ma, respectively (Fig. 6; Mitchell et al. 1983). While the Mte Penoso lavas dip towards the NE, the Malhada Pedra lavas dip towards the SE, indicating that they may originate from a restricted area in the W-central part of Maio. A missing systematic record of dyke directions, as well as faulting and thrusting of units complicates the effort to establish the positions of former eruptive centers. An eruptive center origin in the NW central region of Maio would fit well with a source area from the NW part of the deeper intrusive complex or island core, as deduced from gravity data (Represas et al. 2012), which again implies that this area is a younger part of the CIC. This is consistent with the youngest K–Ar ages (8.6 ± 0.4 Ma and 9.2 ± 0.4 Ma) of CIC intrusive rocks from the Monte Vermelho area (Mitchell et al. 1983). We additionally suggest that flank collapse activity in the Tortonian/Messinian (8.7 to 6.7 Ma) could have enhanced rejuvenated igneous activity of Malhada Pedra and Monte Penoso Formations on Maio, due to decompression-induced melting in the upper mantle.

After the final phase of volcanism (Fig. 7g), erosion was the dominant process shaping Maio. The topography has been flattened and only competent rocks remain as hills (Fig. 7h). Lava flows of the final volcanic phase capped the underlying conglomeratic units, protecting the last remnants from erosion. Quaternary dunes, alluvium and beach sediments are the youngest sediments on Maio.

Conclusions

Based on field observations, structural data and ^{40}Ar–^{39}Ar dating, we can refine the Miocene evolution of Maio Island in the Cabo Verde Archipelago.

Intrusive magmatic growth of Maio probably started in the Early Miocene with the emplacement of shallow plutonic rocks. Edifice growth was dominated by several phases of dyke intrusions and accompanying effusive activity in the Middle Miocene, leading to rapid growth of the island. The associated flare up and uplift is recorded in dyke orientations and resulted in semi-circular dips, deformation and disruption of Mesozoic marine sedimentary successions.

A newly discovered series of conglomerates, interwoven with local pyroclastic units, is interpreted as a flank collapse dominated phase of the Pedro Vaz Formation. The flank collapse events mark a period of rapid erosion in the Tortonian/Messinian (8.7–6.7 Ma), was possibly triggered by tectonic activity (i.e., the Mte Branco Thrust) and corresponds to the onset of rejuvenated volcanic activity. Mass wasting may have induced rejuvenated volcanism of the Malhada Pedra and Monte Penoso Formations due to decompression-induced melting in the upper mantle.

Supplementary Information The online version contains supplementary material available at https://doi.org/10.1007/s00531-022-02160-x.

Acknowledgements The authors would like to thank Thorsten Lux and Karin Junge for help in the labs and with sample preparation. Jan Sticklus is thanked for his invaluable help with ^{40}Ar–^{39}Ar dating of our samples. Dani Bernoulli is thanked for literature, unpublished material and valuable discussions on the geological (stratigraphical) evolution of Maio. Alistair Robertson is thanked for providing literature that was not publicly available. Ricardo Ramalho and Abigail Barker are thanked for their thorough reviews and comments, as well as topic editor Sascha Flögel for his hints, which greatly improved this manuscript. We are grateful for the hospitality and help we received from Dominique Gautherot on Maio, and for logistic help we received from OSCM Mindelo, especially from Cordula Zenk and Ivanice Monteiro. LKS would like to acknowledge financial support from the Helmholtz Research School for Ocean System Science and Technology (HOSST).

Author contributions LKS, THH and WCD: conception and design of the study, field work and sampling; LKS: sample preparation; JAW: ^{40}Ar–^{39}Ar analyses; LKS and JAW: figures and data preparation; LKS, THH, WCD and JAW: interpretation, writing and discussion.

Funding Open Access funding enabled and organized by Projekt DEAL. LKS was supported financially by the Helmholtz Research School for Ocean System Science and Technology (HOSST). The funding source was not involved in the study design, analyses, data interpretation and writing.

Availability of data and material All original data are published in Appendices with this publication.

Code availability N.A.

Declarations

Conflict of interest The authors declare no conflicts of interest.

References

Ali MY, Watts AB, Hill I (2003) A seismic reflection profile study of lithospheric flexure in the vicinity of the Cape Verde Islands. J Geophys Res Solid Earth. https://doi.org/10.1029/2002JB002155

Allmendinger RW, Cardozo N, Fisher DM (2012) Structural geology algorithms. Vectors and tensors. Cambridge University Press, New York, Cambridge, Melbourne

Ancochea E, Huertas MJ, Hernán F, Brändle JL (2010) Volcanic evolution of Sao Vicente, Cape Verde Islands: the Praia Grande landslide. J Volcanol Geotherm Res 198(1–2):143–157. https://doi.org/10.1016/j.jvolgeores.2010.08.016

Annen C, Lénat J-F, Provost A (2001) The long-term growth of volcanic edifices. Numerical modelling of the role of dyke intrusion and lava-flow emplacement. J Volcanol Geotherm Res 105(4):263–289. https://doi.org/10.1016/S0377-0273(00)00257-2

Appel P (2017) Lambert. Geocompass App for iPhone/iPad. Christian-Albrechts University Kiel, Kiel

Azéma J, Fourcade E, de Wever P (1990) Découverte de Valanginien inférieur a Calpionelles à Maio (République du Cap Vert): discussion de l'âge des sédiments associés aux laves de type MORB de ce secteur de l'Atlantique Central. C R Acad Sci Paris Sér IIA 310:277–283

Baksi AK (2007) A quantitative tool for detecting alteration in undisturbed rocks and minerals—I. Water, chemical weathering, and atmospheric argon. In: Foulger GR, Jurdy DM (eds) Plates, plumes and planetary processes, vol 430. Geol Soc Am Spec Pap, pp 285–303

Barker AK, Hansteen TH, Nilsson D (2019) Unravelling the crustal architecture of Cape Verde from the seamount xenolith record. Minerals 9(90):1–13. https://doi.org/10.3390/min9020090

Barker AK, Rydeblad EM, Silva SMDM (2021) Magma storage at ocean islands. In: Masotta M, Beier C, Mollo S (eds) Crustal magmatic system evolution: anatomy, architecture, and physico-chemical processes, vol 264. Wiley-AGU (Geophysical monograph), Hoboke, pp 45–78. https://doi.org/10.1002/9781119564485.ch3

Barrett R, Lebas E, Ramalho R, Klaucke I, Kutterolf S, Klügel A, Lindhorst K, Gross F, Krastel S (2020) Revisiting the tsunamigenic volcanic flank collapse of Fogo Island in the Cape Verdes, offshore West Africa. Geol Soc Lond Spec Publ 500(1):13–26. https://doi.org/10.1144/SP500-2019-187

Begét JE, Kienle J (1992) Cyclic formation of debris avalanches at Mount St Augustine volcano. Nature 356(6371):701–704. https://doi.org/10.1038/356701a0

Bernard B, van Wyk-de-Vries B, Leyrit H (2009) Distinguishing volcanic debris avalanche deposits from their reworked products. The Perrier sequence (French Massif Central). Bull Volcanol 71(9):1041–1056. https://doi.org/10.1007/s00445-009-0285-7

Bernard-Griffiths J, Cantagrel J-M, Matos-Alves C, Mendes F, Serralheiro A, Rocha-de-Macedo J (1975) Données radiométriques potassium-argon sur quelques formations magmatiques des iles de l'archipel du Cap Vert. In: Gauthier-Villards A (ed) Comptes rendus hebdomadaires des séances de l'Académie des sciences. Gauthier-Villars, Paris, pp 2429–2432

Bernoulli D, Hottinger L, Spezzaferri S, Stille P (2007) Miocene shallow-water limestones from São Nicolau (Cabo Verde). Caribbean-type benthic fauna and time constraints for volcanism. Swiss J Geosci 100(2):215–225. https://doi.org/10.1007/s00015-007-1224-2

Cardozo N, Allmendinger RW (2013) Spherical projections with OSX-Stereonet. Comput Geosci 51:193–205. https://doi.org/10.1016/j.cageo.2012.07.021

Carracedo JC (1999) Growth, structure, instability and collapse of Canarian volcanoes and comparisons with Hawaiian volcanoes. J Volcanol Geotherm Res 94(1–4):1–19. https://doi.org/10.1016/S0377-0273(99)00095-5

Cassidy M, Trofimovs J, Watt SFL, Palmer MR, Taylor RN, Gernon TM, Talling PJ, Le Friant A (2014) Multi-stage collapse events in the South Soufrière Hills, Montserrat as recorded in marine sediment cores. In: Wadge A, Robertson R, Voight B (eds) The eruption of Soufrière Hills Volcano, Montserrat from 2000 to 2010, vol 39. Geological Society, London, pp 383–397

Cassidy M, Watt SFL, Talling PJ, Palmer MR, Edmonds M, Jutzeler M, Wall-Palmer D, Manga M, Coussens M, Gernon T, Taylor RN, Michalik A, Inglis E, Breitkreuz C, Le Friant A, Ishizuka O, Boudon G, McCanta MC, Adachi T, Hornbach MJ, Colas SL, Endo D, Fujinawa A, Kataoka KS, Maeno F, Tamura Y, Wang F (2015) Rapid onset of mafic magmatism facilitated by volcanic edifice collapse. Geophys Res Lett 42(12):4778–4785. https://doi.org/10.1002/2015GL064519

Casson M, Bulot LG, Jeremiah J, Redfern J (2020) Deep sea rock record exhumed on oceanic volcanic islands. The Cretaceous sediments of Maio Cape Verde. Gondwana Res 81:252–264. https://doi.org/10.1016/j.gr.2019.11.007

Clague DA, Dalrymple GB (1987) The Hawaiian–Emperor volcanic Chain. Part 1, geologic evolution. In: Decker R, Wright TL, Stauffer PH (eds) Volcanism in Hawaii, vol 1350. US Geol Surv Prof Pap, Hawaii, pp 5–54

Cornu M-N, Paris R, Doucelance R, Bachélery P, Bosq C, Auclair D, Benbakkar M, Gannoun A-M, Guillou H (2021) Exploring the links between volcano flank collapse and the magmatic evolution of an ocean island volcano: Fogo Cape Verde. Sci Rep 11(1):17478. https://doi.org/10.1038/s41598-021-96897-1

Courtney RC, White RS (1986) Anomalous heat flow and geoid across the Cape Verde Rise. Evidence for dynamic support from a thermal plume in the mantle. Geophys J R Astr Soc 87(3):815–867. https://doi.org/10.1111/j.1365-246X.1986.tb01973.x

Crough ST (1982) Geoid height anomalies over the Cape Verde Rise. Mar Geophys Res 5(3):263–271. https://doi.org/10.1007/BF00305564

Dash BP, Ball MM, King GA, Butler LW, Rona PA (1976) Geophysical investigation of the Cape Verde Archipelago. J Geophys Res Solid Earth 81(29):5249–5259. https://doi.org/10.1029/JB081i029p05249

Day SJ, Heleno da Silva S, Fonseca JFBD (1999) A past giant lateral collapse and present-day flank instability of Fogo, Cape Verde Islands. J Volcanol Geotherm Res 94(1–4):191–218. https://doi.org/10.1016/S0377-0273(99)00103-1

de Paepe P, Klerkx J, Hertogen J, Plinke P (1974) Oceanic tholeiites on the Cape Verde Islands: petrochemical and geochemical evidence. Earth Planet Sci Lett 22:347–354

Di Vincenzo G, Viti C, Rocchi S (2003) The effect of chlorite interlayering on ^{40}Ar-^{39}Ar biotite dating: an ^{40}Ar-^{39}Ar laser-probe and TEM investigations of variably chloritized biotites. Contrib Mineral Petrol 145(6):643–658. https://doi.org/10.1007/s00410-003-0472-z

Fleck RJ, Calvert AT, Coble MA, Wooden JL, Hodges K, Hayden LA, van Soest MC, Du Bray EA, John DA (2019) Characterization of the rhyolite of Bodie Hills and ^{40}Ar/^{39}Ar intercalibration with Ar mineral standards. Chem Geol 525:282–302. https://doi.org/10.1016/j.chemgeo.2019.07.022

Fossilworks.org Paleobiology Database Fossilworks. http://fossilworks.org/bridge.pl?a=home. Accessed 25 Mar 2019

Fourcade E, Azéma J, de Wever P, Busnardo R (1990) Contribution à la datation de la croûte océanique de l'Atlantique central: age valanginien inférieur des basalts océaniques et âge néocomien des calcaires Maiolica de Maio (Iles du Cap Vert). Mar Geol 95:31–44

Gradstein FM (2012) The geologic time scale 2012. Elsevier, Amsterdam

Grunau HR, Lehner P, Cleintuar MR, Allenbach P, Bakker G (1975) New radiometric ages and seismic data from Fuerteventura (Canary Islands), Maio (Cape Verde Islands), and Sao Tomé (Gulf of Guinea). In: Borradaile GJ (ed) Progress in geodynamics. Koninklijke Nederlandse Akademie van Wetenshappen, Amsterdam, pp 90–118

Heath M, Phillips D, Matchan EL (2018) An evidence-based approach to accurate interpretation of ^{40}Ar/^{39}Ar ages from basaltic rocks. Earth Planet Sci Lett 498:65–76. https://doi.org/10.1016/j.epsl.2018.06.024

Hunt JE, Wynn RB, Masson DG, Talling PJ, Teagle DAH (2011) Sedimentological and geochemical evidence for multistage failure of volcanic island landslides. A case study from Icod landslide on north Tenerife, Canary Islands. Geochem Geophys Geosys 12(12):Q12007. https://doi.org/10.1029/2011GC003740

Hunt JE, Wynn RB, Talling PJ, Masson DG (2013) Turbidite record of frequency and source of large volume (>100 km^3) Canary Island landslides in the last 1.5 Ma. Implications for landslide triggers and geohazards. Geochem Geophys Geosys 14(7):2100–2123. https://doi.org/10.1002/ggge.20139

Hunt JE, Cassidy M, Talling PJ (2018) Multi-stage volcanic island flank collapses with coeval explosive caldera-forming eruptions. Sci Rep 8(1):1146. https://doi.org/10.1038/s41598-018-19285-2

Kervyn M, Ernst GGJ, van Wyk-de-Vries B, Mathieu L, Jacobs P (2009) Volcano load control on dyke propagation and vent distribution. Insights from analogue modeling. J Geophys Res Solid Earth 114(B3):517. https://doi.org/10.1029/2008JB005653

Klügel A, Hansteen TH, Galipp K (2005) Magma storage and underplating beneath Cumbre Vieja volcano, La Palma (Canary Islands). Earth Planet Sci Lett 236(1–2):211–226. https://doi.org/10.1016/j.epsl.2005.04.006

Klügel A, Longpré M-A, García-Cañada L, Stix J (2015) Deep intrusions, lateral magma transport and related uplift at ocean island volcanoes. Earth Planet Sci Lett 431:140–149. https://doi.org/10.1016/j.epsl.2015.09.031

Koppers A (2002) ArArCALC—software for ^{40}Ar/^{39}Ar age calculations. Comput Geosci 28(5):605–619. https://doi.org/10.1016/S0098-3004(01)00095-4

Lancelot Y, Seibold E, Cepek P, Dean WE, Eremeev VV, Gardner J, Jansa LF, Johnson D, Krasheninnikov V, Pflaumann U, Rankin JG, Trabant P, Bukry D (1978) Site 368: Cape Verde Rise. In: Lancelot Y, Seibold E (eds) DSDP. US Government Printing Office, pp 253–326

Lanphere MA, Dalrymple GB (1978) The use of ^{40}Ar/^{39}Ar data in evaluation of disturbed K–Ar systems. US Geol Surv Open-File Rep 78–701:141–148

Le Bas TP, Masson DG, Holtom RT, Grevemeyer I (2007) Slope failures of the flanks of the southern Cape Verde Islands. In: Lykousis V, Locat J, Sakellariou D (eds) Submarine mass movements and their consequences. 3 International Symposium. Springer, Dordrecht, pp 337–345

Lodge A, Helffrich G (2006) Depleted swell root beneath the Cape Verde Islands. Geology 34(6):449. https://doi.org/10.1130/G22030.1

Ludwig K (2011) User's Manual for Isoplot 4.15. A Geochronological Toolkit for Microsoft Excel 4:77

Madeira J, Ramalho RS, Hoffmann DL, Mata J, Moreira M, Costa P (2020) A geological record of multiple Pleistocene tsunami inundations in an oceanic island. The case of Maio Cape Verde. Sedimentology 67(3):1529–1552. https://doi.org/10.1111/sed.12612

Manconi A, Longpre M-A, Walter TR, Troll VR, Hansteen TH (2009) The effects of flank collapses on volcano plumbing systems. Geology 37(12):1099–1102. https://doi.org/10.1130/G30104A.1

Marques FO, Hildenbrand A, Zeyen H, Cunha C, Victória SS (2020) The complex vertical motion of intraplate oceanic islands assessed in Santiago Island Cape Verde. Geochem Geophys Geosys 21(3):2429. https://doi.org/10.1029/2019GC008754

Martínez-Moreno FJ, Monteiro Santos FA, Madeira J, Pous J, Bernardo I, Soares A, Esteves M, Adão F, Ribeiro J, Mata J, Brum da Silveira A (2018) Investigating collapse structures in oceanic

islands using magnetotelluric surveys. The case of Fogo Island in Cape Verde. J Volcanol Geotherm Res 357:152–162. https://doi.org/10.1016/j.jvolgeores.2018.04.028

Masson DG, Le Bas TP, Grevemeyer I, Weinrebe W (2008) Flank collapse and large-scale landsliding in the Cape Verde Islands, off West Africa. Geochem Geophys Geosys 9(7):Q07015. https://doi.org/10.1029/2008GC001983

McEwen AS, Malin MC (1980) Dynamics of Mount St. Helens' 1980 pyroclastic flows, rockslide-avalanche, lahars, and blast. J Volcanol Geotherm Res 37(3–4):205–231. https://doi.org/10.1016/0377-0273(89)90080-2

McGuire WJ (1996) Volcano instability. A review of contemporary themes. Geol Soc Lond Spec Publ 110(1):1–23. https://doi.org/10.1144/GSL.SP.1996.110.01.01

Mitchell JG, Le Bas MJ, Zielonka J, Furnes H (1983) On dating the magmatism of Maio, Cape Verde Islands. Earth Planet Sci Lett 64:61–76

Montanari D, Bonini M, Corti G, Agostini A, Del Ventisette C (2017) Forced folding above shallow magma intrusions: Insights on supercritical fluid flow from analogue modelling. J Volcanol Geotherm Res 345:67–80. https://doi.org/10.1016/j.jvolgeores.2017.07.022

Nemec W, Steel RJ (1984) Alluvial and coastsal conglomerates: their significant features and some comments on gravelly mass-flow deposits. In: Koster EH, Steel RJ (eds) Sedimentology of Gravels and Conglomerates, Memoir 10, pp 1–31

Pim J, Peirce C, Watts AB, Grevemeyer I, Krabbenhoeft A (2008) Crustal structure and origin of the Cape Verde Rise. Earth Planet Sci Lett 272(1–2):422–428. https://doi.org/10.1016/j.epsl.2008.05.012

Ramalho RS (2011) Building the Cape Verde Islands. Springer Theses. Springer, Berlin, Heidelberg

Ramalho RS, Helffrich G, Schmidt DN, Vance D (2010a) Tracers of uplift and subsidence in the Cape Verde archipelago. J Geol Soc 167(3):519–538. https://doi.org/10.1144/0016-76492009-056

Ramalho RS, Helffrich G, Cosca M, Vance D, Hoffmann D, Schmidt DN (2010b) Episodic swell growth inferred from variable uplift of the Cape Verde hotspot islands. Nat Geosci 3(11):774–777. https://doi.org/10.1038/NGEO982

Ramalho RS, Helffrich G, Cosca M, Vance D, Hoffmann D, Schmidt DN (2010c) Vertical movements of ocean island volcanoes: Insights from a stationary plate environment. Mar Geol 275(1–4):84–95. https://doi.org/10.1016/j.margeo.2010.04.009

Ramalho RS, Quartau R, Trenhaile AS, Mitchell NC, Woodroffe CD, Ávila SP (2013) Coastal evolution on volcanic oceanic islands: a complex interplay between volcanism, erosion, sedimentation, sea-level change and biogenic production. Earth-Sci Rev 127:140–170. https://doi.org/10.1016/j.earscirev.2013.10.007

Ramalho RS, Winckler G, Madeira J, Helffrich GR, Hipólito A, Quartau R, Adena K, Schaefer JM (2015) Hazard potential of volcanic flank collapses raised by new megatsunami evidence. Sci Adv 1(9):e1500456. https://doi.org/10.1126/sciadv.1500456

Represas P, Catalão J, Montesinos FG, Madeira J, Mata J, Antunes C, Moreira M (2012) Constraints on the structure of Maio Island (Cape Verde) by a three-dimensional gravity model. Imaging partially exhumed magma chambers. Geophys J Int 190(2):931–940. https://doi.org/10.1111/j.1365-246X.2012.05536.x

Rigassi DA (1972) Geology and oil prospects of Cabo Verde Islands. Petroconsultants S.A, Geneva

Robertson AHF (1984) Mesozoic deep-water and Tertiary volcaniclastic deposition of Maio, Cape Verde Islands: Implications for Atlantic paleoenvironments and ocean island volcanism. Geol Soc Am Bull 95:433–453. https://doi.org/10.1130/0016-7606(1984)95%3c433:MDATVD%3e2.0.CO;2

Robertson AHF, Bernoulli D (1982) Stratigraphy, facies, and significance of Late Mesozoic and Early Tertiary sedimentary rocks of Fuerteventura (Canary Islands) and Maio (Cape Verde Islands). In: von Rad U, Hinz K, Sarnthein M, Seibold E (eds) Geology of the Northwest African continental margin. Springer, Berlin, Heidelberg, pp 498–525

Romagnoli C, Kokelaar P, Casalbore D, Chiocci FL (2009) Lateral collapses and active sedimentary processes on the northwestern flank of Stromboli volcano Italy. Mar Geol 265(3–4):101–119. https://doi.org/10.1016/j.margeo.2009.06.013

Roverato M, Cronin S, Procter J, Capra L (2014) Textural features as indicators of debris avalanche transport and emplacement, Taranaki Volcano. Geol Soc Am Bull 127(1–2):3–18. https://doi.org/10.1130/B30946.1

Samrock LK, Dullo W-C, Hansteen TH (2018) Large-scale fossil dune on Maio. Cape Verdes Int J Earth Sci (geol Rundsch) 107(8):2931–2932. https://doi.org/10.1007/s00531-018-1622-x

Samrock LK, Wartho J-A, Hansteen TH (2019) ^{40}Ar-^{39}Ar geochronology of the active phonolitic Cadamosto Seamount, Cape Verde. Lithos 344–345:464–481. https://doi.org/10.1016/j.lithos.2019.07.003

Serralheiro A (1970) Geologia da ilha de Maio (Cabo Verde). Junta de Investigações do Ultrama, Lisboa

Stahlecker R (1934) Neocom auf der Kapverden-Insel Maio. N Jb Geol Paläont 73(2):265–301

Steiger RH, Jäger E (1977) Subcommission on geochronology. Convention on the use of decay constants in geo- and cosmochronology. Earth Planet Sci Lett 36(3):359–362. https://doi.org/10.1016/0012-821X(77)90060-7

Stillman CJ, Furnes H, Le Bas MJ, Robertson AHF, Zielonka J (1982) The geological history of Maio, Cape Verde Islands. J Geol Soc 139(3):347–361. https://doi.org/10.1144/gsjgs.139.3.0347

Torres P, Silva LC, Serralheiro A, Tassinari C, Munhá J (2002) Enquadramento geocronológico pelo método K/Ar das principais sequências vulcano-estratigráficas da Ilha do Sal—Cabo Verde Garcia Da Orta. Série Geol 18(1/2):9–13

Urlaub M, Petersen F, Gross F, Bonforte A, Puglisi G, Guglielmino F, Krastel S, Lange D, Kopp H (2018) Gravitational collapse of Mount Etna's southeastern flank. Sci Adv 4(10):eaat9700. https://doi.org/10.1126/sciadv.aat9700

Valderrama Murillo P (2016) Origin and dynamics of volcanic debris avalanches: surface structure analysis of Tutucapa volcano (Peru). Doctoral Thesis, Université Blaise Pascal

van Wyk-de-Vries B, Davies T (2015) Landslides, debris avalanches, and volcanic gravitational deformation. In: Sigurdsson H (ed) Encyclopedia of volcanoes, 2nd edn. Academic Press, San Diego, pp 665–685

van Wyk-de-Vries B, Delcamp A (2015) Volcanic debris avalanches. In: Davies T, Shroder JF (eds) Landslide hazards, risks, and disasters. Elsevier Science, Amsterdam, pp 131–157

Wade BS, Pearson PN, Berggren WA, Pälike H (2011) Review and revision of Cenozoic tropical planktonic foraminiferal biostratigraphy and calibration to the geomagnetic polarity and astronomical time scale. Earth-Sci Rev 104(1–3):111–142. https://doi.org/10.1016/j.earscirev.2010.09.003

Watt S, Talling P, Hunt J (2014) New insights into the emplacement dynamics of volcanic island landslides. Oceanography 27(2):46–57. https://doi.org/10.5670/oceanog.2014.39

Wilson DJ, Peirce C, Watts AB, Grevemeyer I, Krabbenhoeft A (2010) Uplift at lithospheric swells – I. Seismic and gravity constraints on the crust and uppermost mantle structure of the Cape Verde mid-plate swell. Geophys J Int 182(2):531–550. https://doi.org/10.1111/j.1365-246X.2010.04641.x